Spring 2017

Anthropometric shape parameters in obese subjects: implications for obese total joint arthroplasty patients

Kevin James Simoens
University of Iowa

ANTHROPOMETRIC SHAPE PARAMETERS IN OBESE SUBJECTS: IMPLICATIONS FOR OBESE TOTAL JOINT ARTHROPLASTY PATIENTS

By

Kevin James Simoens

A thesis submitted in partial fulfillment
of the requirements for the Master of Science
degree in Biomedical Engineering in the
Graduate College of
The University of Iowa

May 2017

Thesis Supervisor: Professor John J Callaghan

Graduate College
The University of Iowa
Iowa City, Iowa

CERTIFICATE OF APPROVAL

MASTER'S THESIS

This is to certify that the Master's thesis of

Kevin J Simoens

has been approved by the Examining Committee for the thesis requirement for the Master of Science degree in Biomedical Engineering at the May 2017 graduation.

Thesis Committee:

John J Callaghan, Thesis Supervisor

Nicole M Grosland

Jacob M Elkins

Donald D Anderson

To my friends and family whom have given me never-ending support while in pursuit of a personal dream.

ACKNOWLEDGEMENTS

First and foremost, I would like to thank my research supervisor Dr. John Callaghan and orthopedics resident Dr. Jacob Elkins for their guidance and continued support during my time with the University of Iowa Hospitals and Clinics Department of Orthopedics. Additionally, I'd like to thank Dr.'s Callaghan and Elkins, and all of those who contributed to the prior research on biomechanics in the obese population for their substantial contributions. Also, I would like to thank Dr. Ruth Chimenti, Connor Dilger, and the Orthopedic Gait Analysis Laboratory for their assistance. Dr. Callaghan provided funding for my research through the Roy D. Crowninshield Biomechanics Endowment Fund. I would also like to thank the Orthopedic Biomechanics Lab, with special thanks to Dr. Don Anderson for furthering my knowledge and skills in the world of orthopedics. In addition, I'd like to thank Dr. Nicole Grosland for her continuous help and advising presence over the last few years. Finally, I'd like to thank my family and friends for their unconditional support.

ABSTRACT

Obesity is a severe concern worldwide and its prevalence is expected to continue to increase. Linked to diabetes, kidney disease, heart disease, and high blood pressure among other things, obesity has been identified as the forthcoming, largest preventable cause of mortality. Osteoarthritis, surgical consequences, distribution of subcutaneous adipose tissue, and alteration of joint biomechanics have vast implications in total joint repair (TJR). Previous studies have linked obesity to increased forces through weight-bearing lower extremities, alterations in gait, and risk of implant failure. The objectives of this study were to (1) provide a tool to predict lower extremity dimensions and shape variations of subcutaneous adipose tissue, (2) identify the degree to which obesity influences shape variation of the osseous anatomy of the knee joint, and (3) lay a foundation to compare the knee contact force of obese patients in activities of daily living.

Long-leg EOS films were obtained, retrospectively over 5 years, from 232 patients that were being seen at the Adult Reconstruction Clinic at the University of Iowa. Using custom Matlab algorithms, measurements of soft tissue distribution and lower extremity osseous anatomy were obtained and analyzed. Additionally knee contact force measurements were obtained through motion capture analysis and modeling in Anybody Technology.

Males and females had similar lower extremity shapes, with females having greater knee circumferences than males. The variability of PPT and PTT tended to be greater in females and increased with increasing BMI. Although similar in the anteroposterior direction, males tended to have on average 12mm wider proximal tibias in the mediolateral direction. Clinical observations of increased post-operative complications trend with these findings. The future of research into biomechanics of obesity will rely heavily on anatomic models of the obese lower extremities, which until this work did not exist.

PUBLIC ABSTRACT

Obesity is a severe concern worldwide and its prevalence is expected to further increase. Linked to chronic diseases, obesity has been identified as the soon to be largest preventable cause of mortality. Joint pain, surgical consequences, distribution of fat, and alteration of joint biomechanics have vast implications in total joint repair (TJR). Previous studies have linked obesity to increased forces throughout the legs, alterations in gait, and risk of joint replacement failure. The objective of this study was to construct an anatomical modelling library of obese lower extremities and develop a foundation for computation of obese modelling parameters defining activities of daily living.

Long-leg EOS radiograph films were obtained, retrospectively over 5 years, from 232 patients that were being seen at the Adult Reconstruction Clinic at the University of Iowa. Using custom software, measurements of fat distribution and leg boney anatomy were obtained and analyzed. Additionally knee contact force measurements were obtained through motion capture analysis and modeling in Anybody Technology.

Males and females had similar lower extremity shapes, with females having greater knee circumferences than males. The variability of PPT and PTT tended to be greater in females and increased with increasing BMI. Although similar in the anteroposterior direction, males tended to have on average 12mm wider proximal tibias in the mediolateral direction. Clinical observations of increased post-operative complications trend with these findings. The future of research into biomechanics of obesity will rely heavily on anatomic models of the obese lower extremities, which until this work did not exist.

TABLE OF CONTENTS

LIST OF FIGURES

PREFACE

Obesity is recognized across the globe as a serious problem. It is known to have adverse effects on every organ system, and thus affects all specialties of medicine. Obesity perhaps affects orthopedics more than any other field of medicine. Thousands of articles exist in the orthopaedic literature, which describe adverse complications related to obesity. However, very few studies have attempted to answer why. Fundamental information is severely lacking to serve as a basis to start meaningful investigation into the biomechanics of obesity on the musculoskeletal system.

A long-term objective of the lab is to be able to computationally model total joint replacement in obese subjects. To begin, finite element models are needed. For finite element models, the following parameters must be modelled: joint replacement implants, accurate representation of the osseous anatomy, and lower extremity soft tissue structures. In addition to these parameters, input kinetics (joint contact forces) and input kinematics (joint rotations for use as boundary conditions) must be modelled as well in order to properly load and constrain the model. From examination of prior literature and in-house capabilities, the implant design is a known entity. However, bone geometry, lower extremity geometry, input kinetics, and input kinematics remain as unknowns. To evoke the words of Shakespeare as he wrote “Nothing will come of nothing” [1], we must start somewhere. This work is a start.

CHAPTER 1: PREDICTION OF LOWER EXTREMITY SHAPE FROM BMI IN OBESE POPULATION

1.1: Introduction/Literature Review

Obesity is a serious issue, not only in the United States, but also worldwide, due slightly to genetic factors, but mainly to today's environment [2]. With trends toward continued higher caloric intake, less exercise, and inadequate sleep at the forefront, obesity is expected to only further rise [2]. Obesity is defined as having a body mass index (BMI, weight in kilograms divided by the square of the height in meters) of 30 or greater, with overweight defined by a BMI > 25 [2] [3] [4] [5]. With 33.8% of the U.S. population already defined as obese and 396 million people defined as obese worldwide, it is estimated that by the year 2030, these numbers will be maintained at 33% in the U.S and reach 1.12 billion worldwide [6] [7] [8]. Physiologically, obesity has been linked to hundreds of illnesses and pathologies, including high blood pressure, heart disease, stroke, chronic kidney disease, type-2 diabetes, sleep apnea, osteoarthritis, and gastroesophageal reflux disease [2]. Overweight (BMI > 25) and obese individuals combined account for two-thirds of the U.S. population [9]. A recent study stated that if the increasing trend of being overweight is not reversed over the next few years, poor diet and physical inactivity will likely overtake tobacco as the leading preventable cause of mortality [10], and in fact obesity has already been identified as the largest preventable cause of disease burden in some regions [11].

In the world of biomechanics, increased BMI is associated with alterations in gait, as well as increases in forces throughout the body, especially the weight-bearing lower extremity [12]. These deviations from the normal human motion and loading forces can adversely affect the joints supporting the motion. Obesity has shown such aberrations as decreased range of motion of the knee, increased osteoarthritis, shorter step length, increased wear on joints, and alterations to gait to accommodate larger body mass [13].

Osteoarthritis (OA), affection nearly 27 million Americans, is a degenerative joint disease occurring most often in the weight-bearing joints of the lower extremity, including knees, hips, and lower back. It is characterized by a degeneration of cartilage, causing pain, swelling, and decreased range of motion. When worsened, cartilage can wear away causing bone-to-bone contact and painful joint damage [14]. Although OA is linked more to increased body weight than BMI [15], it is reported that BMI still very strongly correlates with OA (Figure 1) [16]. Obesity also greatly increases the effects of osteoarthritis (OA) in knees, post-operation. When obese patients reduce their weight by as little as 5kg, it is believed that 24% of surgical cases on knee OA could be avoided [17].

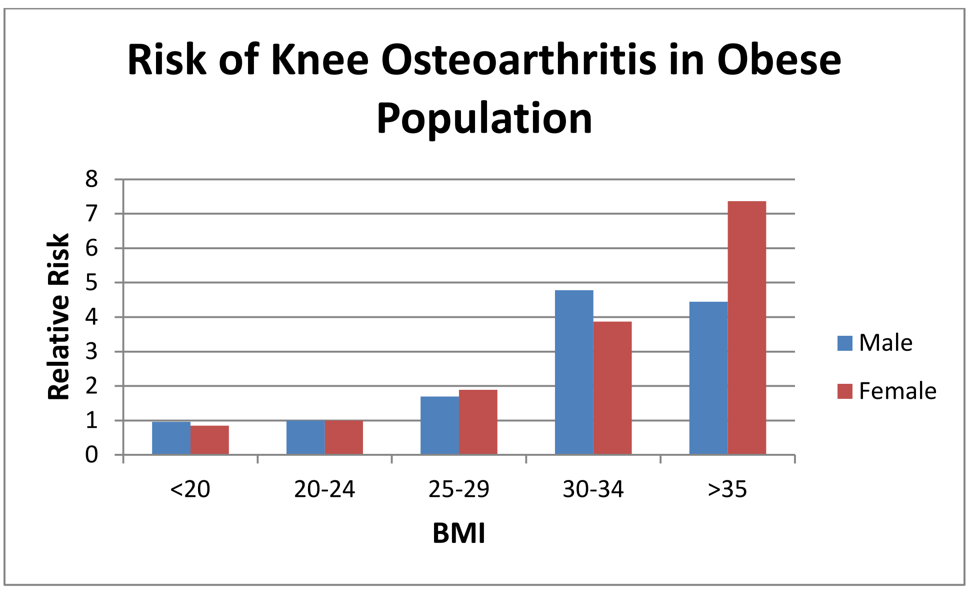

Figure 1: Graph of risk ratios at varying BMI demonstrates that the risk of OA increases nearly exponentially with increasing BMI. Data from [18].

The most definitive treatment modality for end-stage OA is total joint replacement, most commonly total hip and total knee arthroplasty (THA and TKA, respectively). In 2005, approximately 800,000 total hip and knee replacements were performed in the United States. By 2030, it is estimated that the number of primary total hip arthroplasties will reach 572,000 annually and the number of primary total knee arthroplasties will reach 3.48 million annually [6]. Patients with BMI > 40 are 32.73 times as likely to require a TKA during their lifetime as those of a BMI < 25 [19].

As the number of total joint replacements is on the rise, the number of revision operations will rise as well, especially in obese patients. BMI, along with percent body fat are directly associated with increased perioperative risks [20]. In a study by Watts et al., there is a direct association between subcutaneous fat thickness and early reoperation and infection following TKA in morbidly obese (BMI > 40 kg/m^2) patients [21]. The Knee Society Score is a patient-reported outcome measure (on a scale of 1-100) of patient satisfaction and function measured 8-months following total knee arthroplasty. According to a study by Foran et al, 88% of obese patients scored a rating of success (>80) for their knee replacement, much lower than the 99% to reach that mark in the normal weight patients [22]. Most of the “failures” are due to infection, poor wound healing, or mechanical failure, which were all drastically increased in the obese population. Resulting from increased body mass, obese implant survival is plagued by increased wear rates [23]. Obese patients generate greater joint loads due to increased body mass. These loads generate greater frictional forces in implants, increasing rates of abrasion [24]. Altered gait in obese subjects can lead to altered loading patterns in joints, ultimately causing wear in non-weight-bearing locations [25].

In an attempt to better categorize the obese population, investigators have attempted to categorize people into different groups based on their anthropometric differences and study how those groups affect the outcome of total joint arthroplasty. In the literature, categorization of individuals by their adipose deposition and muscle definition is defined by various morphotypes. There are three main morphotypes (Figure 2) including ectomorphs, mesomorphs, and endomorphs.

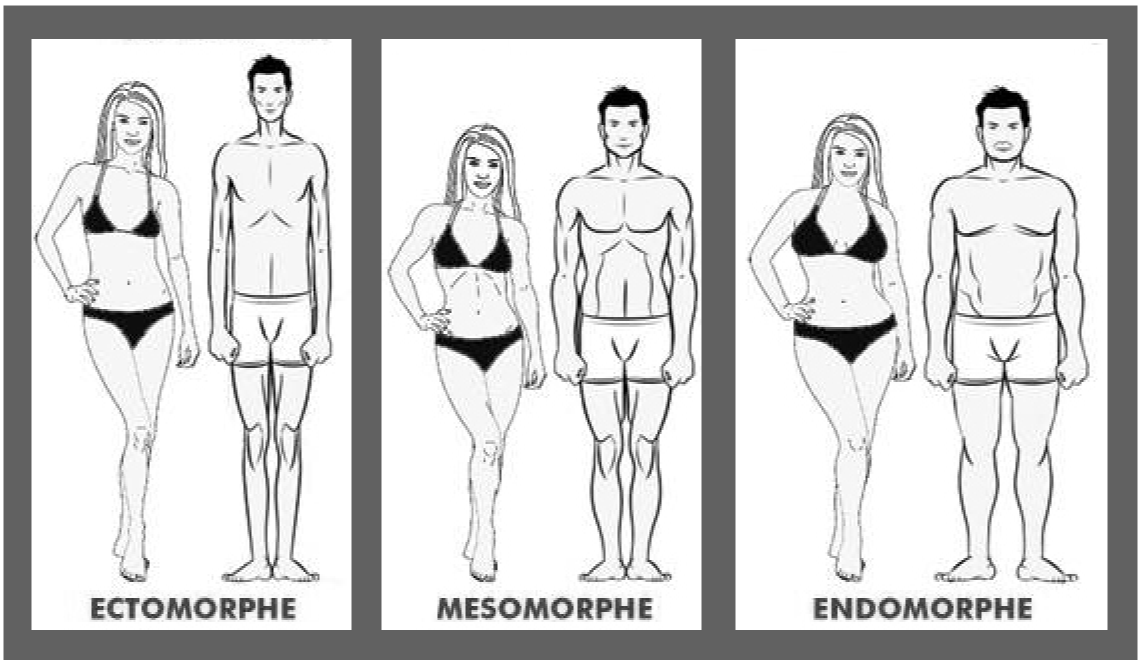

Figure 2: Ectomorphs are characterized by tall, slim figures with narrow hips and shoulders. Mesomorphs are characterized by an "hourglass" figure with medium build, broad hips and shoulders, and a tiny waist. They are generally the most muscularly toned. Endomorphs are characterized by a larger overall body frame, carrying more fat, and having larger bones. Reprinted from [26].

One such categorization – and likely the most well-known – is simply identifying body shape as either "apple" or "pear" shaped based on the location of adipose tissue deposition [27]. Men typically trend more toward the apple shape or a larger chest and stomach with smaller diameter legs, and women typically trend more toward the pear shape with larger waists, thighs, and legs. It is believed that both gender and morphotype play a role in influencing the shape of the knee in patients undergoing TKA [28]. Bellemans et al, using knee CTs and long-leg radiographs, found that females had narrower bones near the knee than males. They also found that patients with short and wide morphotype (endomorph) had wider bones in the knee, whereas patients with the long and narrow morphotype (ectomorph) had more narrow bones in the knee, both regardless of gender.

Another attempt of body shape classification was performed in the South Korean population [29]. Park and Park measured roughly 35 dimensions of nearly 2800 individuals that were considered to be "large" based on either Broca index (BI, ideal weight equal to height in cm minus 100) $\geq$ 20, BMI $\geq$ 25, or waist-to-hip ratio (WHR, circumference of the waist divided by the circumference of the hip) $\geq$ 1.0. A majority of these dimensions were circumferences of common landmarks over the human body. From this data, they divided the individuals into four categories for males, and four for females entitled "Large everywhere", "Small figure but above average legs", "Large torso surface", "Small legs and small torso", and "Large torso and below-average shoulder width", "Wide shoulder and below-average lower body", "Small Torso and large lower body", "Small figure", respectively [29].

Prior studies provide only for qualitative analysis of body shape, which provides limited utility when attempting to advance forward with robust biomechanical studies of the effect of obesity on the musculoskeletal system. In this study, long-leg radiographs were used to generate predictive shaping parameters for the lower extremities of obese patients, based on age, sex, and BMI. The objective of this study is to provide a tool to predict lower extremity dimensions in much more exacting detail than previous investigations.

1.2: Methodology

Data was collected retrospectively from a total of 232 patients with known BMI, age, and sex. Lower body images were obtained, over a course of five years, from patients that were being seen at the Adult Reconstruction Clinic at the University of Iowa. For each patient, images obtained include: two standing long-leg films obtained from an EOS machine (anteroposterior (AP)/lateral views) Figure 3 [30], and two standard AP and lateral radiographs of the knee as seen in Figure 4.

Figure 3: EOS image collection representation. Two low-dose X-ray tubes move vertically, simultaneously capturing biplanar digital images of patient. Radiation beams produce 45cm wide scanning area, resulting in rapid, high quality images with pronounced accuracy and little to no error resulting from source-to-plate angles [30].

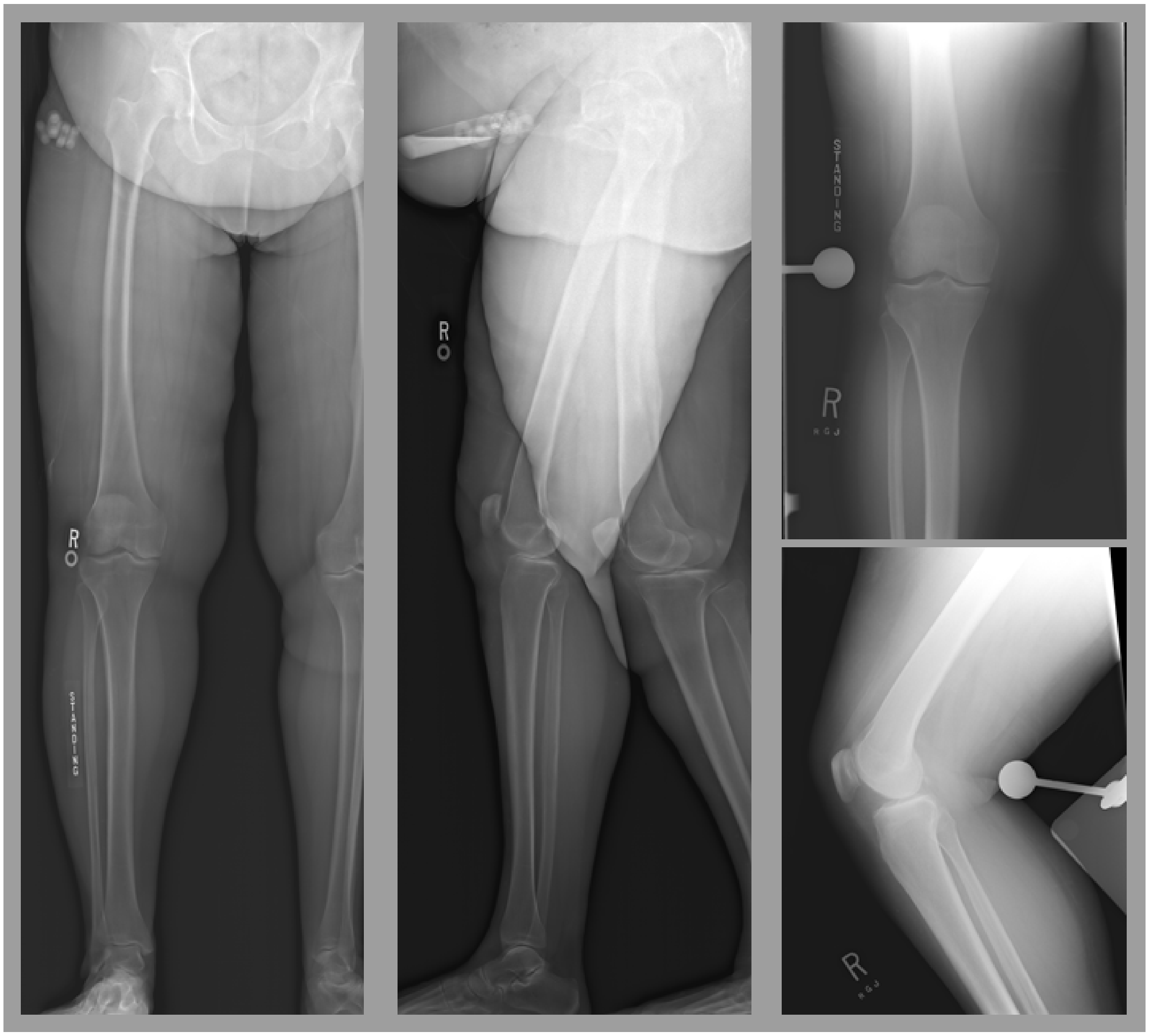

Figure 4: AP and lateral standing long-leg films from EOS machine and standard AP and lateral radiographs of the knee prior to image processing.

A radio-opaque object, or “sizing ball” of known diameter (30.0mm), was included in both of the standard radiographs of the knee. This sizing ball, provided in one image from each plane, along with similar differences between the articulating edge of the patella and the proximal edge of the tibia (Figure 5), were used to calibrate pixel lengths for computation of distances using Matlab [31] [32].

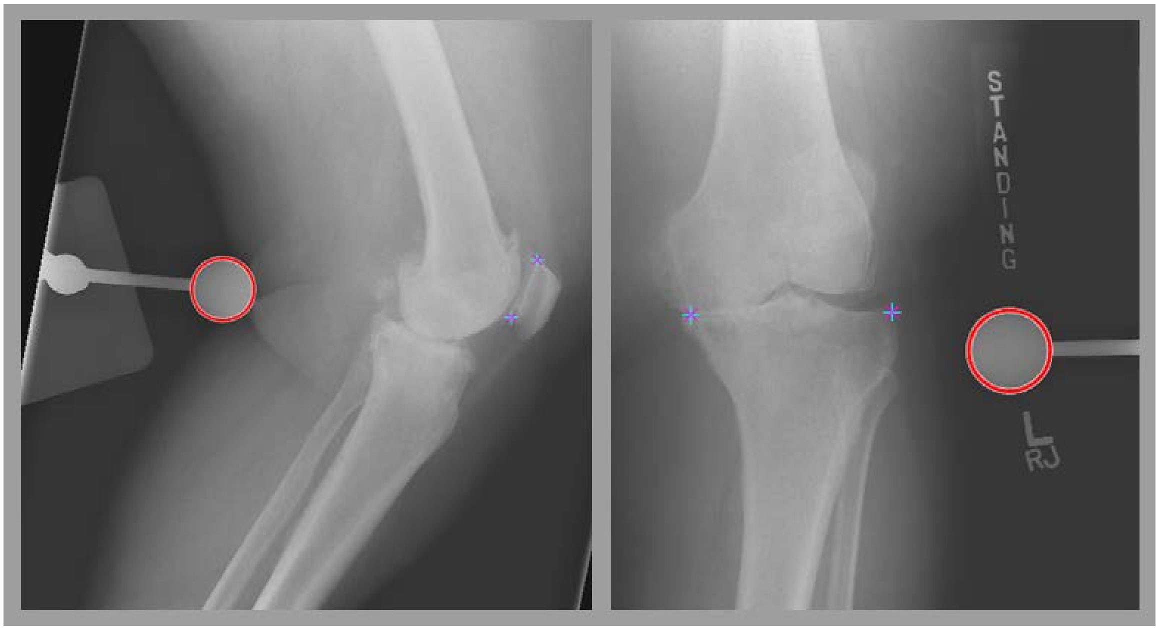

Figure 5: Diameter of sizing ball, along with lengths of the articulating surface of the patella and proximal edge of the tibia were used to calculate pixel lengths for use in distance data collection.

In some cases, bone spurs, or osteophytes, were present in the radiographs, which can impede the measurements and placement of the seed points. When encountered during measurement, protocol was to place the seed points at the location where the tibia would likely be, without the excess bone. An example of a case with bone spurs can be seen in Figure 6. The seed points are represented by the red diamonds and were placed at the intersection of the tibial plateau and the black tibial contour lines.

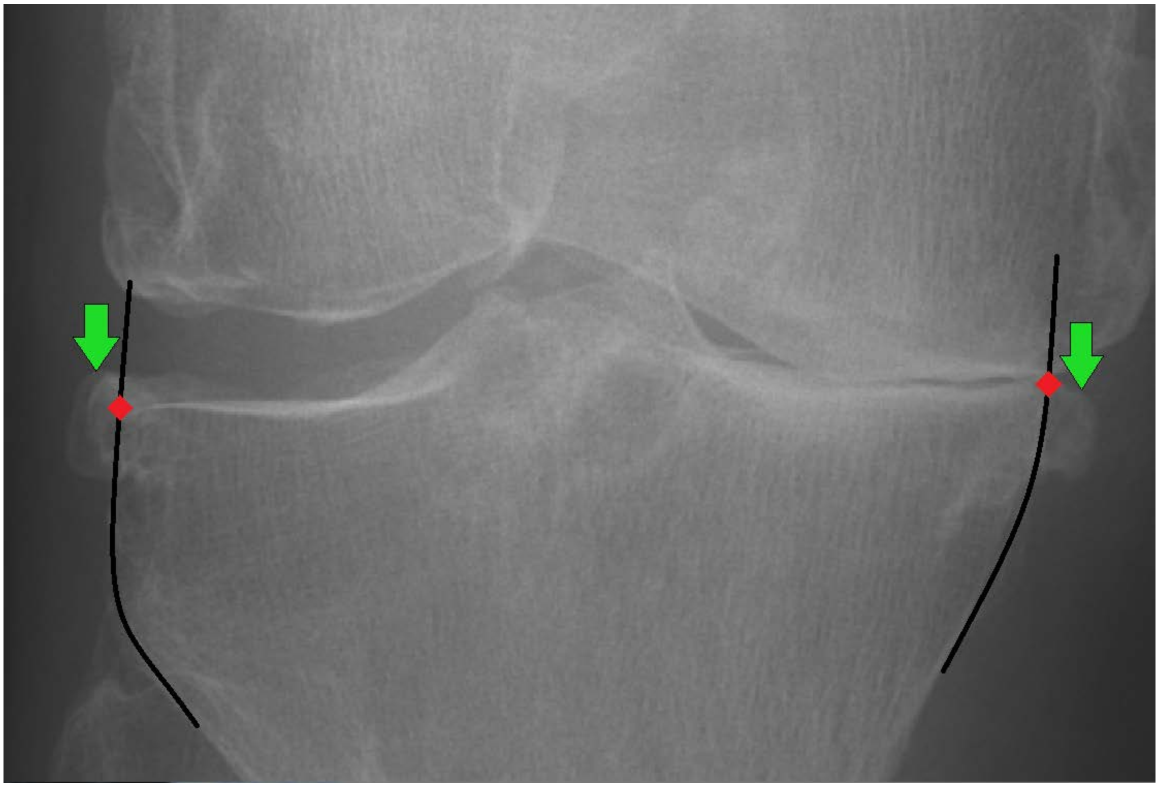

Figure 6: Demonstration of seed point placement in the presence of bone spurs. The black lines align with the contour of the tibia and extend through where the bone edge would be without the bone spurs, pointed out by the green arrows. The seed points were placed at the junction of the tibial plateau and the black lines.

Anatomical curves and lines were generated (Figure 7), through Matlab algorithms, onto the images for use in distance calculations. The femoral curve (femur-bisecting curve approximating the sagittal bow of the femur), femoral line (femur-bisecting curve in the AP plane), and tibial line (bisecting curve in the AP plane) were defined using bony landmarks. Centers of the femoral head, femoral trochanteric region, and talus were found using circles generated by placing three points on the bony surface of each respective region. The femoral curve (in the lateral images) was generated by connecting the center of the femoral head to the distalmost point of the femur, running through a point in the center of the femoral shaft. The femoral curve (in the AP images) was generated by connecting the center of the femoral trochanteric region to the tibial condyle, running through a point in the center of the femoral shaft. The femoral line (in the lateral images) was generated by connecting the femoral head to the distalmost point on the femur. The tibial line was generated by connecting the intercondylar eminence to the center of the talus. Measurements collected consisted of the distances from several points along the outer edge of the thigh and leg to the center of the femur and tibia as can be seen in Figure 7.

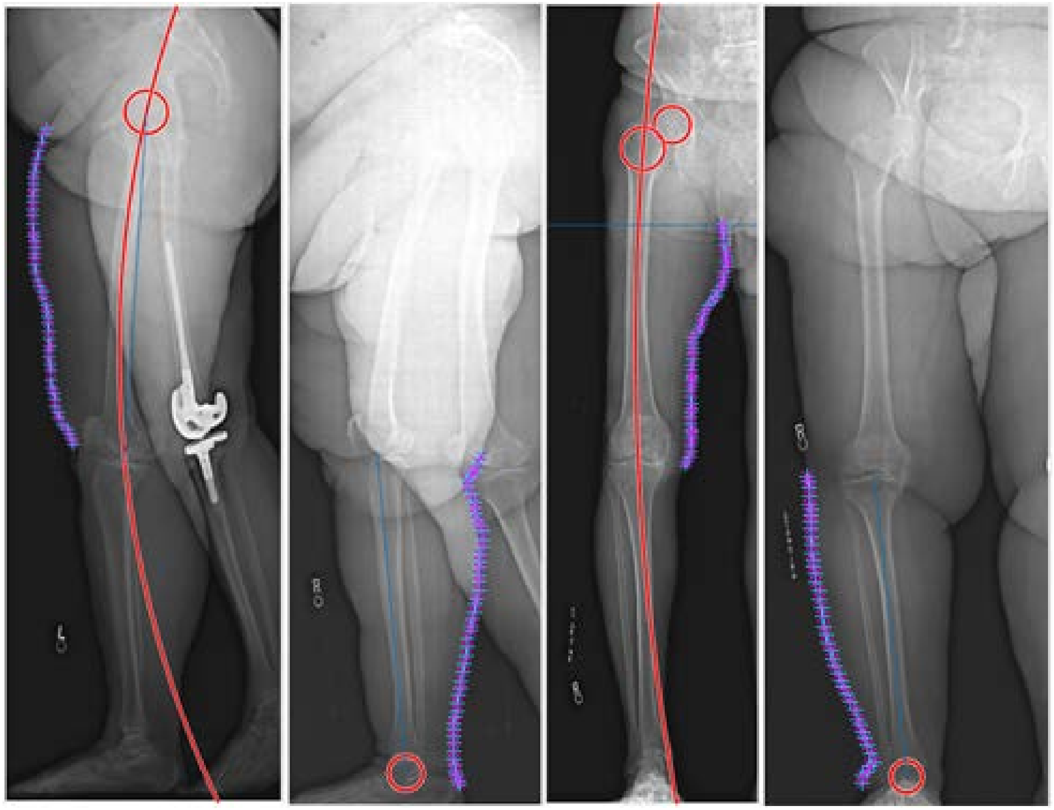

(A) (B) (C) (D)

Figure 7: Screen shots of the MATLAB distance collection interface. (A) In the lateral plane, for each point along the anterior surface of the thigh, a distance, orthogonal to the femoral line, was calculated to the femoral curve, following the contour of the femur. These same lines were used for the posterior region beginning 30% of the way down the femur (30% was chosen as to measure distal from the perineum, which precludes accurate measurement of circumference). (B) Distances for the lower leg were calculated from each point, anteriorly and posteriorly, to its orthogonal counterpart on the tibial line, passing through the center of the tibia. (C) In the coronal plane, again the orthogonal distances from each point to the femoral curve at the center of the femur were recorded, beginning at the height of the center of the femoral head and 25% down the thigh from the center of the femoral head for the lateral and medial surfaces respectively. (D) As in the lateral view, the distances for the lower leg were calculated from each point to its orthogonal counterpart on the tibial line, both laterally and medially.

The measurements were assessed for reproducibility by re-running 15 of the patients, selected at random, a second time and comparing their data to the original measurements in an attempt to reduce intra-observer variability. All surface-to-bone length measurements averaged ± 2mm (range, ± 8mm) difference from their original measurement. Once recorded from MATLAB, the distances, x-y coordinates of each point, and bone length were loaded into MathCAD for further data analysis. For each patient, splines were created for the four skin measures data points: medial, lateral, anterior, and posterior. Each spline was written as a function of distance down the lower extremity (separated by leg and thigh). Thus for any position along the leg, four points can be computed. Another program was written in MathCAD to directly solve, via eigenvectors, the least-error fit coefficients for a best-fit ellipse through these four points [33] [34], generating values for a, b, x_0 and y_0 (Figure 8). The general equation for an ellipse [35]:

$$\frac{(x - x_0)^2}{a^2} + \frac{(y - y_0)^2}{b^2} = 1$$

Values for all patients were then statistically averaged based on BMI. From this data, plots comparing BMI, age, sex, and leg circumference were created.

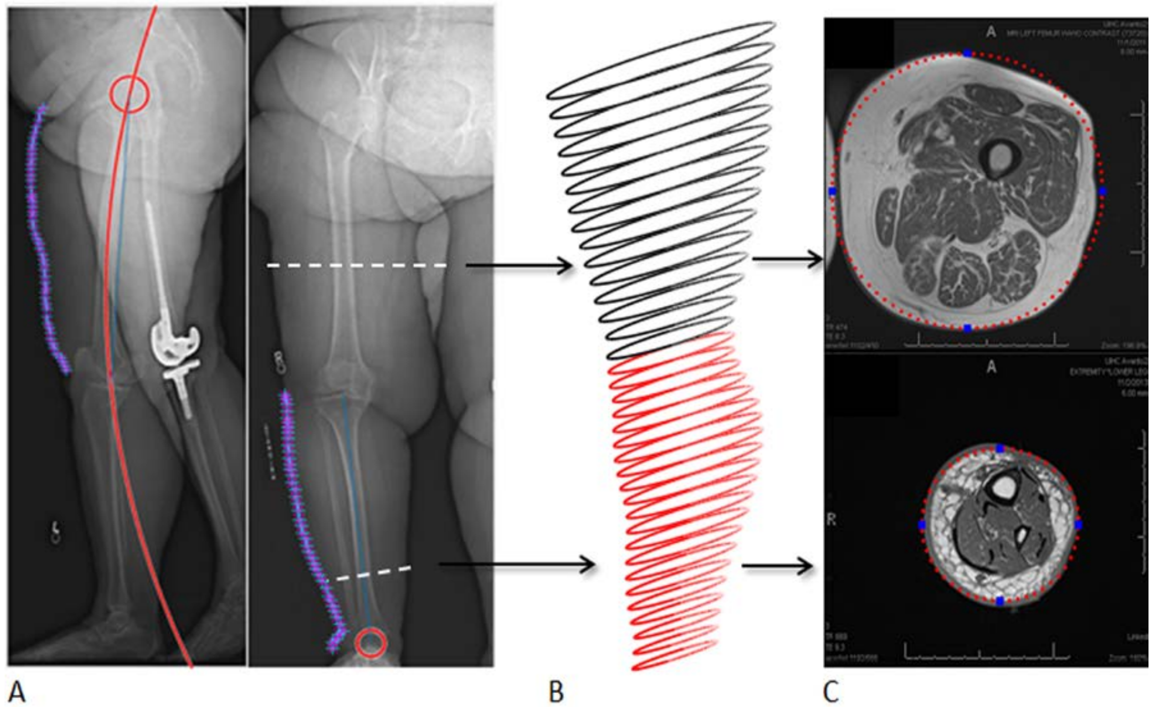

Figure 8: Computational algorithm (A) generates fitted ellipses for any cross-section along the lower extremity (B). Good fit and correlation is seen with MRI validation.

1.3: Results

Lower extremity girth increased with increased BMI. While overall distributions of adipose tissue varied between males and females (Figure 9), maximal girth was comparable between the two groups. In general anteroposterior distribution was more sensitive to BMI than adipose tissue distribution in the mediolateral directions.

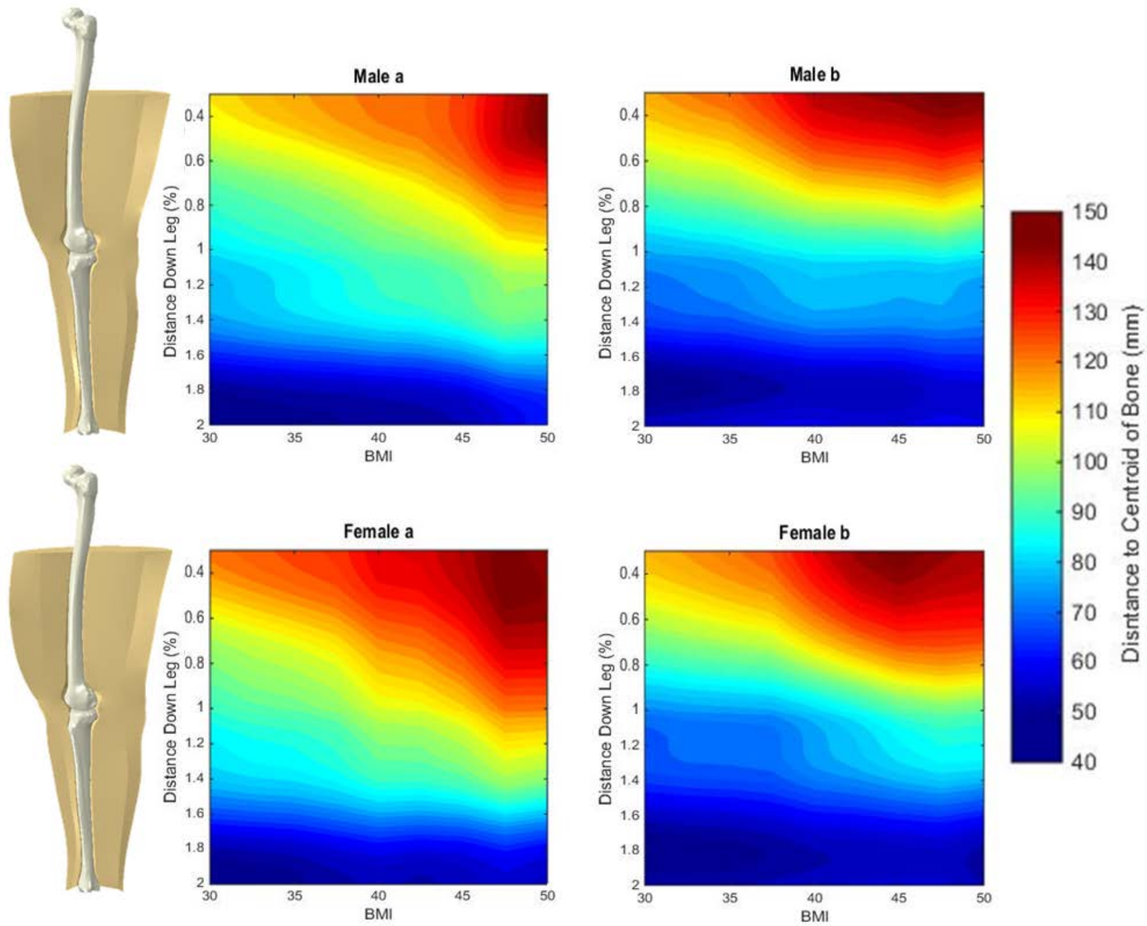

Figure 9: Contour plots showing the distance from soft tissue surface to center of bone based off BMI and distance down the leg. Major (a), coinciding with the ML direction, and minor (b), coinciding with the AP direction, axes for the fitting ellipse are shown as a function of BMI for male (top) and female (bottom) subjects.

In general, females demonstrated slightly larger thighs across all BMI categories. One noteworthy finding is that approaching the knee from proximal to distal, the difference between male size and female size becomes much more appreciable, especially with increasing BMI. This same observation is observed when approaching the knee from distal to proximal. Plots of these variations can be viewed in Figure 10 and Figure 11.

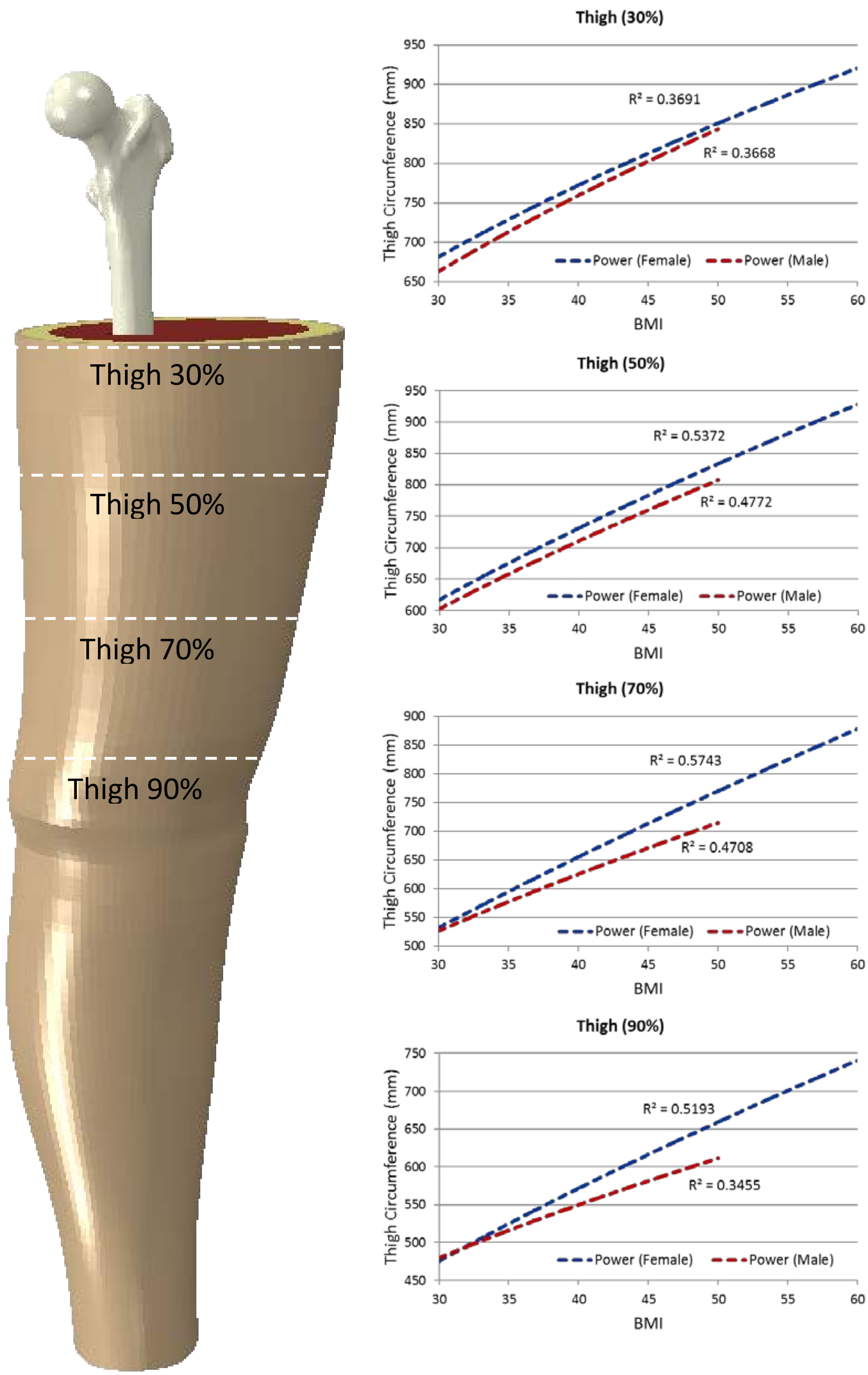

Figure 10: Comparison of thigh circumference between males and females across varying BMIs.

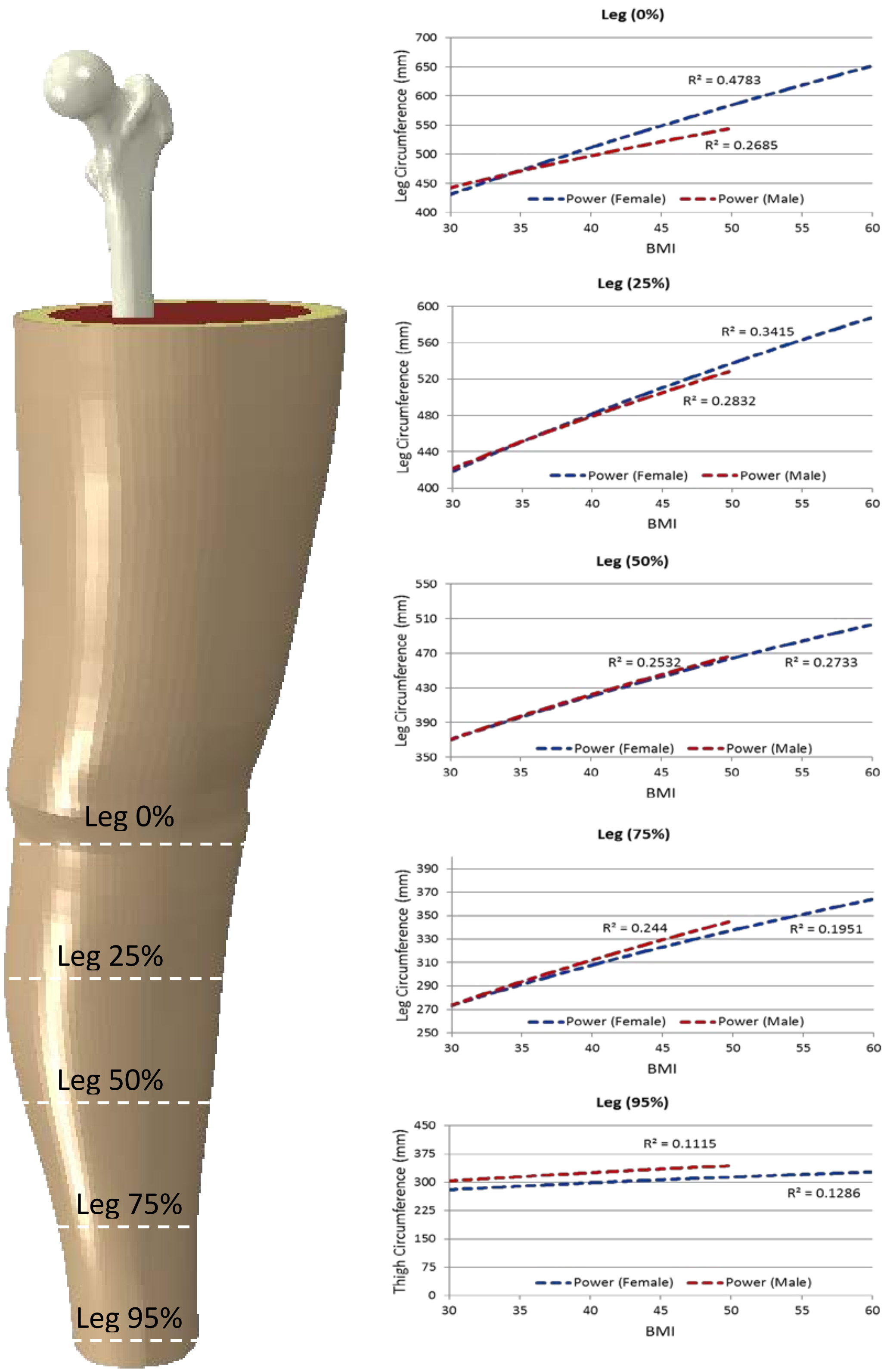

Figure 11: Comparison of leg circumference between males and females across varying BMIs.

Table 1: Demonstration of the coefficients of determination for each of the plots in Figures 10&11.

R^2-Values	Distance Down Extremity	Female	Male
Thigh	30%	0.3691	0.3668
	50%	0.5372	0.4772
	75%	0.5743	0.4708
	90%	0.5193	0.3455
Leg	0%	0.4783	0.2685
	25%	0.3415	0.2832
	50%	0.2733	0.2532
	75%	0.1951	0.244
	95%	0.1286	0.1115

The coefficients of determination in Table 1 above show that the lower extremity circumference tends to vary more in males than in their female counterparts. Also, it is observed that BMI better correlates with circumference in females than in males and better correlates in both sexes around the mid-thigh region (50-75%) than it does around the gluteal sulcus (thigh-30%) or the ankle (leg-95%).

1.4: Discussion

Contrary to the simplistic morphotype analysis of body shape, this study delineates the lower extremity body shape in much greater detail, providing quantitative analysis of lower extremity shape based on BMI, sex, and age. Observing Figure 8, one is able to gather detailed information about the soft tissue distribution in both the anteroposterior direction as well as the mediolateral direction of the leg by solely knowing the patient's BMI and sex. As seen in Figure 10 and Figure 11, males and females had similar lower extremity shapes, with males having slightly lower thigh circumferences, but the knee region showed a lot of variation in shape with females having much greater knee circumferences than males. These results perhaps corroborate the clinical observation of greater risk of post-operative wound complications in obese females versus their male counterparts. Wound healing complications and deep infection rates increase with larger BMI [36]. Fluid can collect in the dead space between the skin and extensor mechanism during TKA in obese patients. Typically, surgeons apply a negative-pressure wound vacuum in at-risk areas to prevent fluid pooling, but still fluid may collect, resulting in pressure on skin closure, preventing proper wound healing [37]. Adipose tissue prevents adequate oxygenation throughout tissue, causing higher rate of infection and poor wound healing [38]. Patients with BMI > 40 demonstrated nearly twice the risk of hospital wound problems, as well as nearly three times the rate of deep infections following TKA compared to non-obese patients [39]. Additionally, the larger circumference of the lower extremity in obese patient has also been implicated in greater risk for component malpositioning and prosthesis loosening [40] [38].

As demonstrated in this present study, both BMI and sex strongly influence lower extremity limb shape. This perhaps carries implications regarding patient-specific implant designs, agreeing with previously reported thoughts that both sex and body shape need to be taken into account for implant design [28]. Possible alterations in high BMI individuals include increased thickness of polyethylene tray to offset increased propensity for accelerated wear, longer and wider tibial stems to increase the bending rigidity of the implant and allow for better fixation, and wider tibial components to increase the surface area between the implant and tibia in order to lower stress.

The lower extremity shape prediction demonstrated here can be used to generate accurate representations of lower extremity adipose distribution on a patient specific basis. Accurate quantification of leg shape and adipose tissue variability is important for determining variability in both native knee and total knee replacement kinematics. This is important not only for permitting precise computational assessment of the joint biomechanics in obese patients, but also to predict possible adverse outcomes following TKA. This study considerably expands our knowledge-base of lower extremity shape in obese patient beyond simple morphotype analysis. Thus in reference to the long-term goals of the lower extremity model, the extremity geometry is now a known entity.

There were a few limitations in this study. Using patients with end-stage OA requiring TKA, the patient population was limited, which made it difficult to conclude significant findings. The patient population was also condensed around the BMI-35 mark. For better quantification, further analysis with a wider range of BMIs, including non-obese BMIs would have been useful. Also, because the measurements recorded were strictly distance of soft tissue, there was no differentiation between varying types of firm or soft fat. Another limitation was the contrast of a small number of the images, as some boney landmarks were difficult to decipher.

CHAPTER 2: SUBCUTANEOUS FAT THICKNESS AS A PREDICTOR OF LOWER EXTREMITY VARIANCE IN OBESE PATIENTS

2.1: Introduction/Literature Review

Obesity has long been associated with adverse outcomes following TKA. Alignment in any joint replacement is more difficult in obese patients, in part because of the adipose tissue obstructing bony landmarks, limiting visual field, and disabling the surgeons to place alignment devices properly. Thus the use of computer navigation is being used more, especially in TKA [41]. In women, BMI has been associated with medial meniscus body extrusion due to increased loads [42]. In a previous study, patients with BMI $\geq$ 35 had increased risk of tibial component loosening [43]. Another study demonstrated that BMI was significantly associated with increased rates of reoperation, revision surgery, incidence of wound infection, and deep infections [44] [45]. Furthermore, obesity has been shown to be a risk factor for adverse outcomes in other fields of surgery: In colorectal surgery, surgical site infection increases with obesity [46]. Subcutaneous fat thickness is also correlated to increased rates of surgical site infection following cervical spine fusion [47]. Obese patients have significantly greater risks (2% to 3.3%) of thromboembolic events such as deep vein thrombosis or pulmonary embolisms [48].

Other studies have demonstrated that adverse outcomes in TKA may not be as dependent on BMI as the actual adipose distribution. One study measured BMI, limb length, suprapatellar, and infrapatellar limb girths in a group of BMI $\geq$ 35 TKA candidates, finding that BMI was not associated with tourniquet time (a surrogate for surgical time); however, short limbs with elevated suprapatellar girth increased tourniquet time and surgical complexity [49]. Patient time of exposure is often increased and inabilities to evert the patella were 27.2 times greater in patients where thigh girth was greater than 55cm [50] [51]. During TKA in obese patients, the extra adipose tissue can cause dead space where fluid can collect, placing additional pressure on skin closure, which can increase wound complications [37].

Examining tissue distribution around the knee, measurements of prepatellar thickness (PPT) and pretubercular thickness (PTT) have been used to correlate tissue distribution to joint complications. Commonly found in basketball players, carpenters, and obese individuals (people who kneel often or place extreme loads on the knee), prepatellar bursitis is an inflammation of the bursa lying anterior to the patella. This tissue becomes inflamed due to knee trauma by either an acute instance (jumping in basketball) or trauma over time (extensive loading on the knee in obese patients) [52]. In early 2016, Watts et al. correlated early complications in TKA patients living with morbid obesity (BMI $\geq$ 40) to amount of subcutaneous fat tissue. He showed this with the two measurements of prepatellar subcutaneous PPT and PTT [21]. The PPT was measured as the distance between the midpatella and the point where the perpendicular bisector of the anterior patella meets the skin surface. The PTT was measured as the distance between the outermost prominent aspect of the tibial tubercle and the skin surface, with the measurement perpendicular to the anterior cortex of the tibial tubercle (Figure 12). Defining a complication as a reoperation for poor wound healing or infection within 90 days of the primary operation, Watts et al. calculated risk ratios of 2.0 for PPT $\geq$ 15mm, 1.6 for PTT $\geq$ 25mm, and 1.0 for BMI $\geq$ 50kg/m^2; thus concluding that local fat distributions may be a better indicator of wound complication than BMI.

Figure 12: Measurements of PPT and PTT as used by Watts et al [21].

Previous studies have associated PPT and PTT metrics to early reoperation and infection after TKA in morbidly obese patients. These studies compared matched patient groups to test only for correlation with post TKA outcomes. However, this study compares the variance of PPT and PTT for each sex across the obesity spectrum.

2.2: Methodology

Using the same patient population and images from Chapter 1, a custom Matlab algorithm was used to calculate the prepatellar thickness (PPT) and the pretubercular thickness (PTT) from the two standard radiographs of the knee. The Matlab code used a Hough transform as an edge detector to find locate the sizing ball and calculate its diameter. A function was then programmed to zoom in on the knee so that accurate placement of the seed points could be assured. After generating the points for the PPT measurement, the system zoomed in on the proximal third of the tibia to assure accurate selection of the tibial seed points. From the zoomed lateral knee radiographs, the thickness of the soft tissue in both the prepatellar and pretubercular regions were measured (Figure 13) in accordance with the methodology by Watts et al and were automatically output to an excel file for processing [21]. Complete PPT and PTT measurements could be obtained in 231 patients. The measurements were tested for reproducibility as in section 1.2 of Chapter 1. All length measurements averaged +/-1mm (range, +/-3mm) difference from their original measurement.

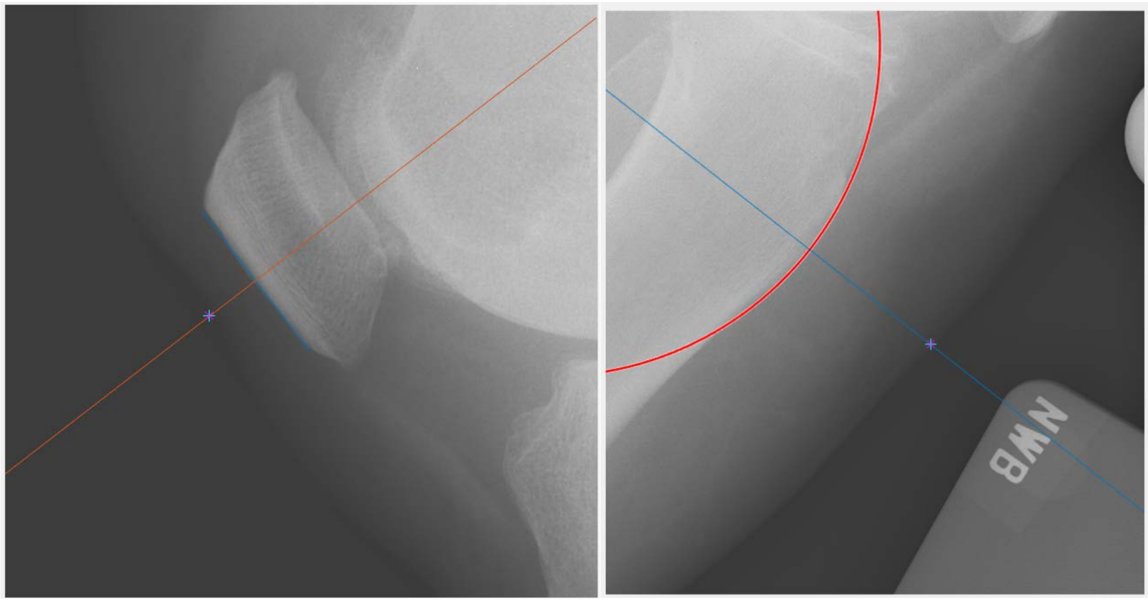

(A) (B)

Figure 13: Screen shots of the MATLAB soft tissue measurement interface. (A) Using two seed points, the anterior-patellar line was constructed to line the anterior surface of the patella. From that line, a perpendicular bisector was constructed (patellar bisector) expanding the length of the image. The soft tissue measurement was taken as the distance from the point at which the patellar bisector intersects with the tissue surface, to the point at which the same patellar bisector intersects with the anterior-patellar line on the surface of the patella. (B) Using three seed points, two along the anterior surface of the tibia, one below and one above the tubercle, and the third point along the curvature of the tubercle, an arch was generated to contour the surface of the tubercle (tubercular curve). Originating from the center of the curve and passing through the surface of the tubercle, a radial line was constructed orthogonal to the anterior surface of the tubercle. The soft tissue measurement was taken as the distance from the point at which the radial line intersects with the tissue surface, to the point at which the same radial line intersects with the anterior surface of the tubercle (tubercular curve).

2.3: Results

With the average age slightly greater for males (63.9 yrs. for male; 63.1 yrs. for female), the female population demonstrated greater mean BMI, PPT, and PTT. For the measurements of BMI, PPT, and PTT, males averaged 36.7kg/m^2, 9.19mm, and 7.79mm respectively; the females averaged 38.24kg/m^2, 12.79mm, and 20.00mm respectively. Even when the population was controlled for BMI, females demonstrated significantly greater adiposity on average both at the knee ($p = 0.000176$) and slightly below the knee ($p = 9.07 \times 10^{-15}$). These comparisons are demonstrated in Figure 14.

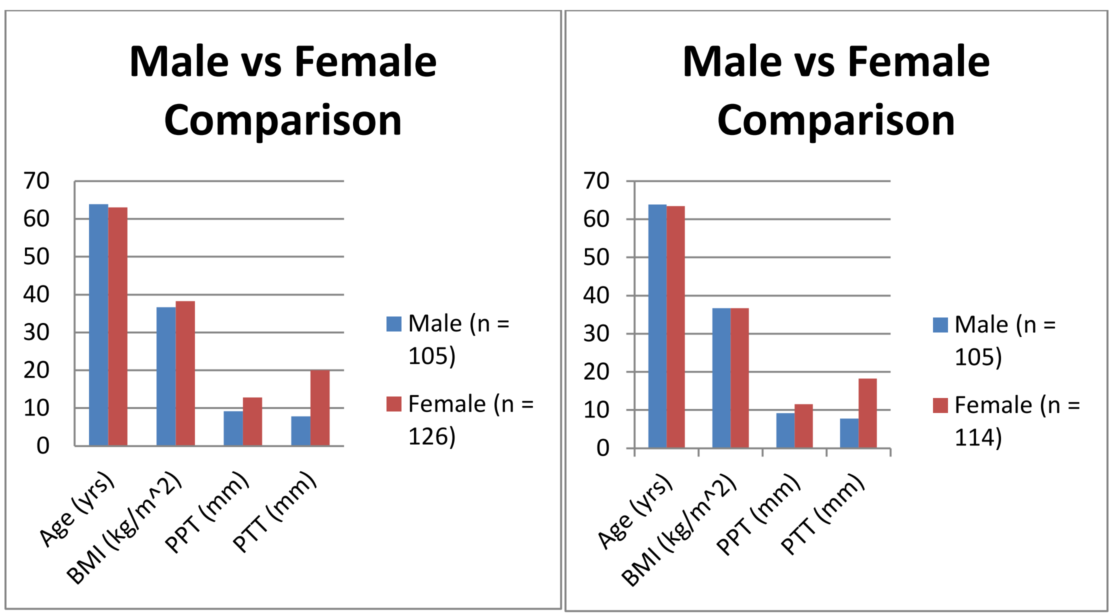

(A) (B)

Figure 14: Charts show the average age, BMI, PPT, and PTT for males and females. (A) Demonstrates a comparison among the entire patient population. (B) Demonstrates a comparison among a population controlled for BMI. This population, generated to look at the differences in PPT and PTT when the average BMI was constant, was formed by eliminating the most distant outliers until the average BMI was matched.

The female patients trended toward an increase in both PPT and PTT with increased BMI, whereas the males demonstrated a fairly constant thickness across the BMI spectrum (Figure 15). Also, females demonstrated greater variance than males in PPT and PTT across all BMI groups. While the male population increased variance slightly with increasing BMI in the PPT, females increased variance greatly with increasing BMI for both PPT and PTT (Figure 16).

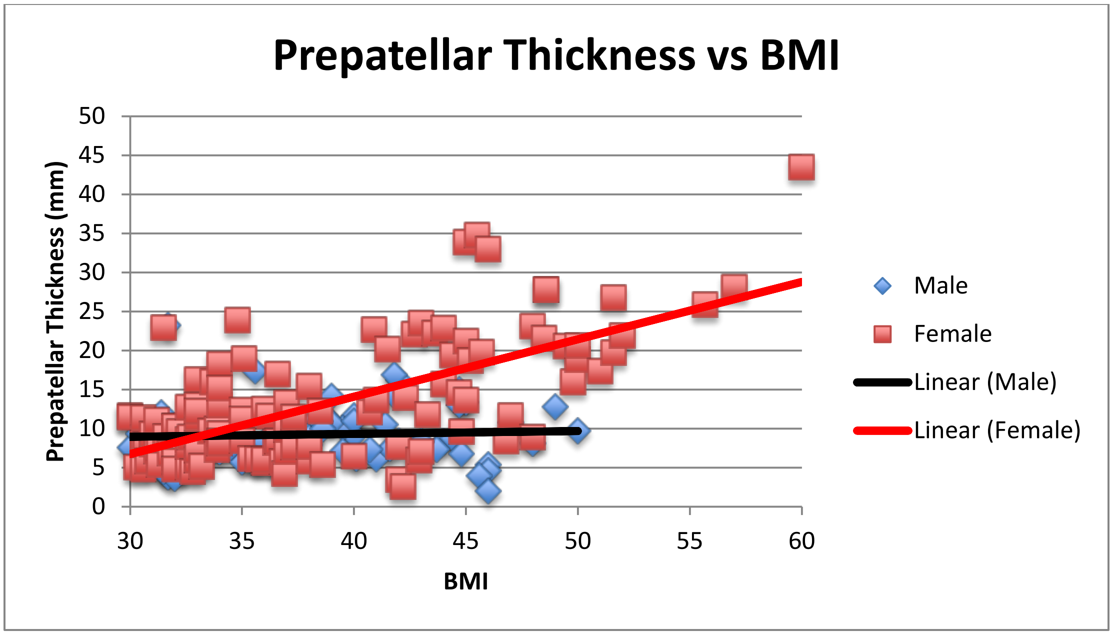

(A)

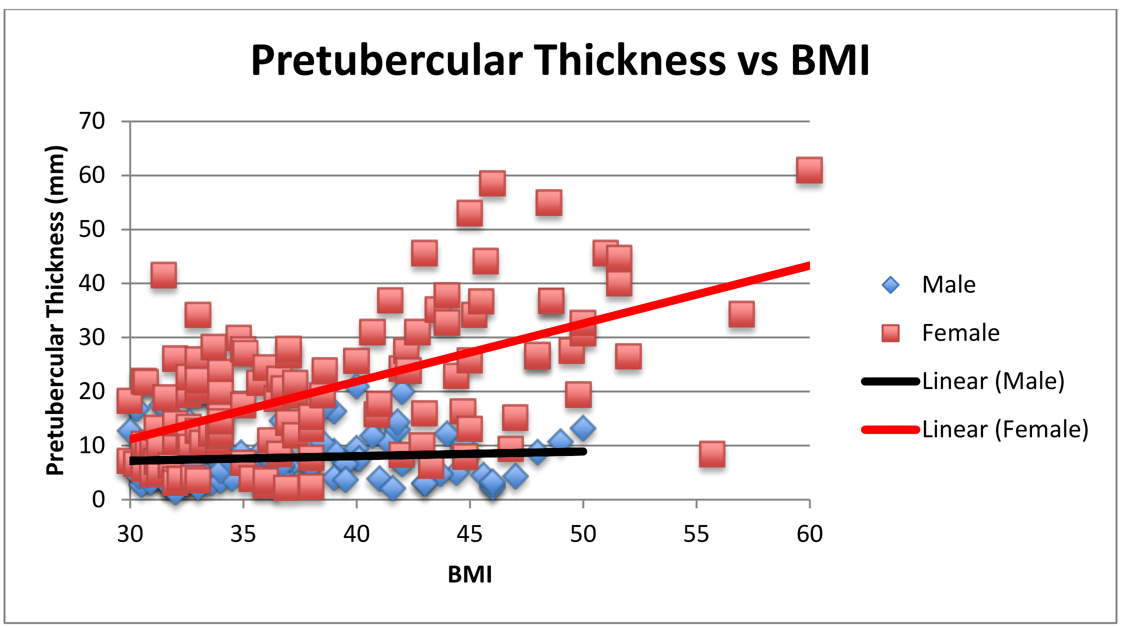

(B)

Figure 15: (A) Demonstrates a comparison between PPT and BMI for males and for females. (B) Demonstrates a comparison between PTT and BMI for males and for females.

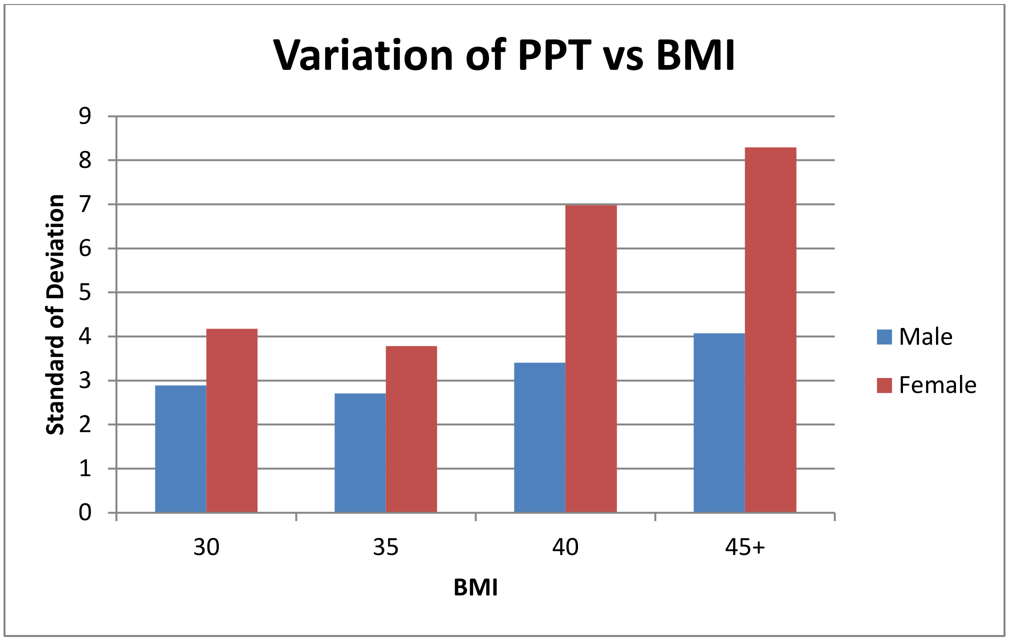

(A)

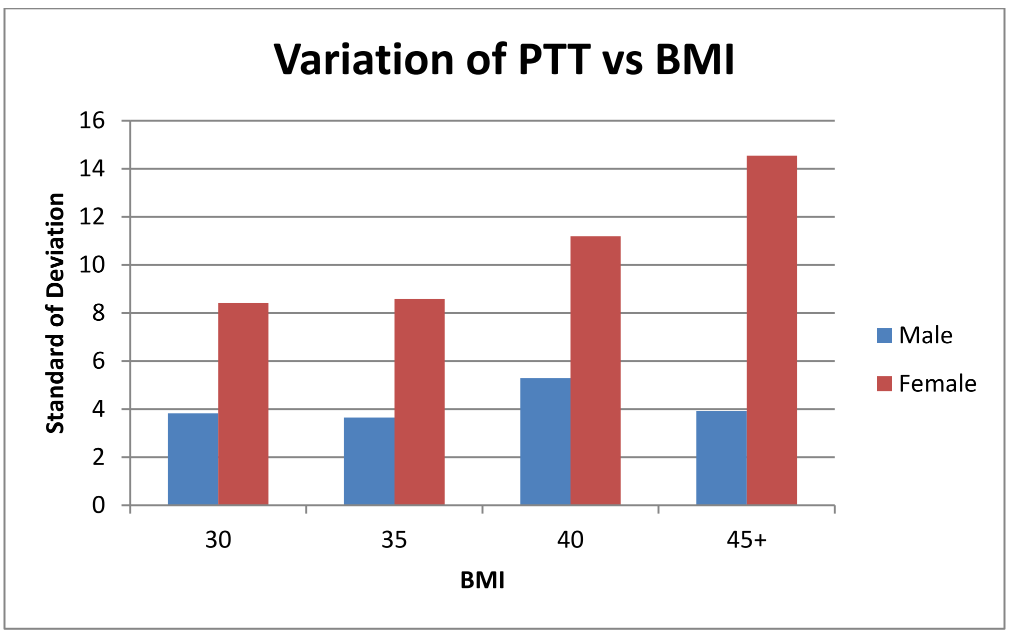

(B)

Figure 16: The graph shown in (A) shows, by standard of deviation, that female PPT varied much more than that of males, especially with increasing BMI. (B) Shows that female PTT varies much more than that of males and varies more with increasing BMI.

2.4: Discussion

The female population overall had higher average subcutaneous fat thicknesses in the prepatellar and pretubercular regions. BMI also seemed to have more of an effect on increased adipose thickness in women than it did in men, as the average thickness in males remained relatively unchanged with increasing BMI. In Figure 16, the female population had greater variability in all BMI groups, for both PPT and PTT. An interesting finding was that the variability of thickness in females trended to increase with increasing BMI, whereas in males, the variance remained relatively steady with increasing BMI.

These results were as expected based on previous body shape categorization methods, generalizing anthropometric body shapes into “apple and pear” categorizations based on the location and types of fat storage. Males more often demonstrate central obesity, carrying their weight in their chest and stomach regions with thinner legs, while females tend to demonstrate a greater propensity toward peripheral obesity, depositing more fat tissue into their hips, thighs, and legs [27]. While overall girth is important to surgeons, thickness of adipose tissue at the surgical site is of particular interest because greater thickness of tissue has been linked to many complications. Increased risk of local infection, deep infection, wound complications due to poor blood flow and increased dead space, and component malpositioning have all been associated with greater adipose tissue thickness at the surgical site [39] [40] [38]. In Watts et al.’s analysis of complications due to fat tissue, they found that the complications were much more related to the thickness of tissue than the overall BMI of the individual. They demonstrated markedly increased complications for PPT $\geq$ 15mm and PTT $\geq$ 25mm [21]. When referencing Figure 15, it is apparent that many subjects approach or exceed these at-risk thicknesses, across a wide spectrum of patient BMIs. An obvious avenue for further investigation will include clinical review of this patient cohort to identify local adipose tissue thicknesses predisposing to wound complications or other adverse post-operative events. Additionally, further investigation should be conducted on finding if different surgical techniques would be better for patients with more variable tissue thicknesses; this may include design of new prosthesis alignment devices that are more patient specific based on tissue distribution instead of overall BMI. Additionally, in reference to the long-term goals of the lower extremity model, the extremity geometry is now a known in greater detail.

CHAPTER 3: TIBIAL REGION VARIATION IN OBESE PATIENTS

3.1: Introduction

Obesity has been strongly associated with early and accelerated weight-bearing joint degeneration due to increased/abnormal loading on those joints. Increased body weight contributes to increased wear within the skeletal structure [53]. In load-bearing joints, increased body mass increases joint contact forces [54]. Many studies have demonstrated that increased implant loads secondary to an increase in body weight also increase wear rates leading to aseptic loosening as a result of osteolysis [55] [56]. In mechanics, the stress on an object is a function of the force per unit of area. Therefore, in biomechanics, the stress on a joint is a function of the force on the joint per unit of area of the joint. As previously demonstrated, large forces (secondary to increased body weight) on tibias of small cross-sectional area can fail catastrophically due to overloading the bearing surface and collapsing in varus [57]. Thus a joint with greater loading, as in an obese person, would demonstrate decreased joint contact forces in the setting of increased load-bearing area [58].

Wolff's law states that bone, mainly bone mineral density, in healthy individuals will adapt to the loads under which it is placed. Bone should remodel in response to strain stimuli in order to mechanically reduce stress [59]. However, it is important to note that bone may not remodel by increasing size, thus increasing surface area to decrease the stress. Most remodeling is accomplished in terms of altering bone mineral density, increasing density in areas of high stress. When comparing tibia shape in a group of 143 cadaveric limbs, it was found that although the AP diameter of the shaft increases in obese subjects, there were no other significant size differences in the tibia between normal and obese subjects [60]. When comparing body mass to bone morphology, there is a relationship between an increases cross-sectional diameter of the shaft. However, while cross sectional shaft strength predicts body mass well, it can be much more difficult to measure reliably than an articular breadth (cross-sectional area of proximal tibia) [61].

A simplistic free-body diagram (Figure 17) of the tibial surface (red) demonstrates the idea behind increasing the area of the joint in order to lower stress. As studies have shown, bone in obese patients show increased tibial shaft diameters as demonstrated from (A) to (B). This remodeling will help the strength of the bone throughout the shaft. However, contact surface at which the load is applied stays the same size; therefore with increased body mass, the stress will rise. When designing an implant, in an attempt to reduce stress, the joint surface area can be enlarged (C), which can combat the greater forces being applied in obese individuals. Another way to reduce the stress of an implant is to increase the length of the stem, transferring the load over a larger area. Some tibial components have been designed with greater congruity in order to increase surface area for reduction of stress and enhancing stability [62]. These implants, however, possess less joint mobility, and also lead to increased interfacial strain secondary to increased implant constraint, thereby possibly leading to increased rates of implant loosening.

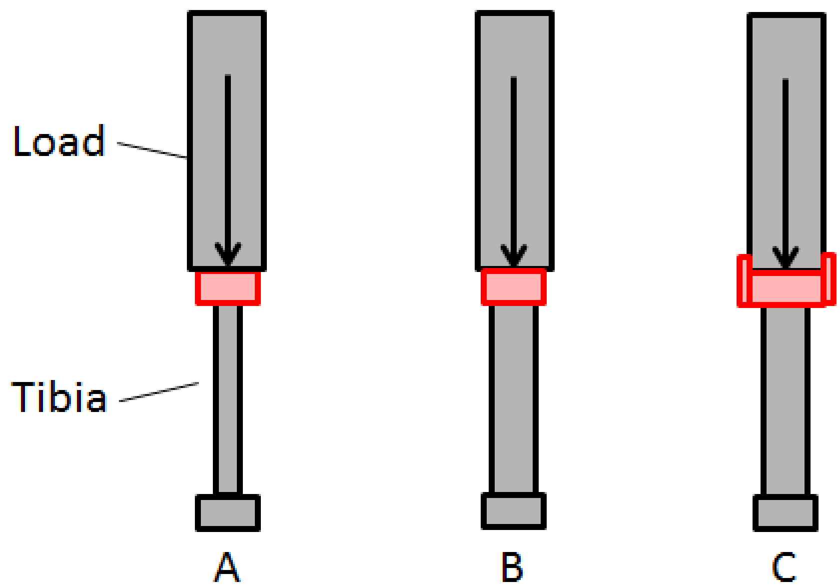

Figure 17: If equal forces are applied on in all three cases, (A) represents a load being placed on a tibia, (B) represents how the tibia would increase its shaft diameter, but not the size of the proximal tibia, and (C) represents how the bone or implant should theoretically respond in order to reduce stress in the knee joint.

An important metric in the anteroposterior physiology of the knee is thought to be the tibial anterior slope. Anatomic studies have identified a normal tibial posterior slope of the lateral plateau of approximately 6-7 degrees (Figure 18). Alterations from this can lead to aberrant joint loading, potentially leading to accelerated joint degeneration, tissue and ligament tear, tibial subluxation, and dislocation [63] [64] [65].

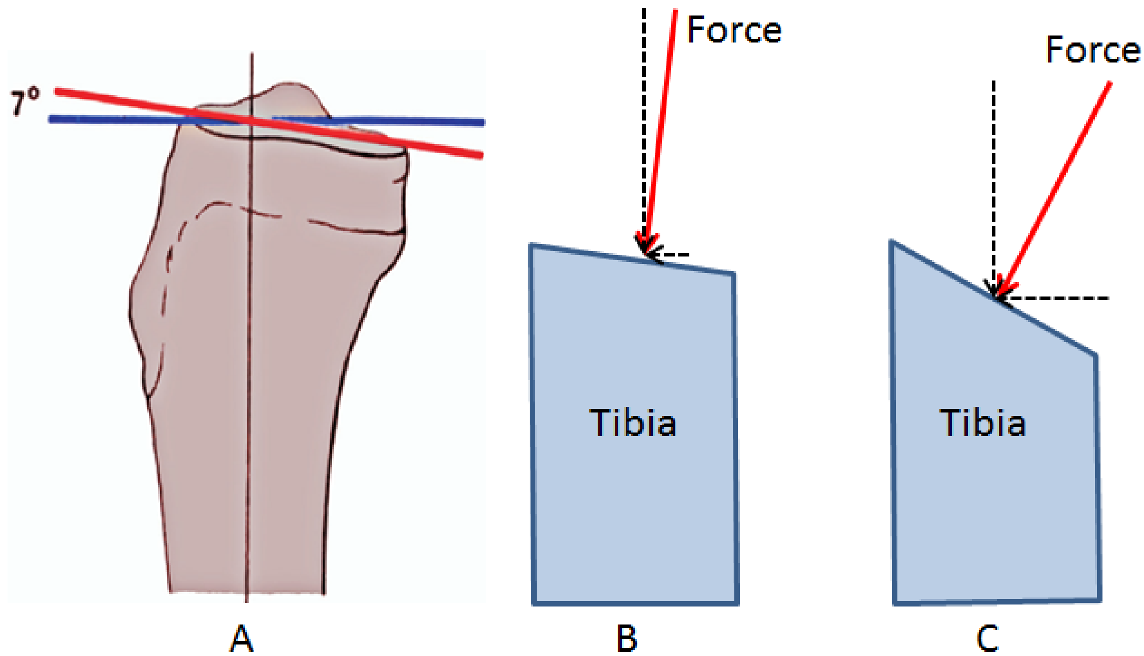

Figure 18: Anterior tibial slope is defined as the angle between the line perpendicular to the tibial shaft and the inclination of the tibial plateau (A, reprinted from [64]). The inclination line is normally taken with respect to the lateral condyle. When the tibial slope is small, the normal force us directed mainly through the mechanical axis of the tibia (B). When the tibial slope is larger, the horizontal component becomes more of a factor, sometimes causing anterior tibial migration (C).

In the coronal view, variations in the varus or valgus deformation of the leg can play a large role in alterations in gait, stresses, and stability of the knee [66]. In TKA, the knee is typically aligned to create an anatomic alignment of approximately 5-7 degrees of valgus to obtain the normal tibiofemoral angle and optimize stability and flexibility [67]. It is important to recognize the different alignment methods in the lower extremities when comparing measurements (Figure 19). The mechanical axis is determined by drawing a line from the center of the femoral head to the center of the ankle joint and represents the direction of loads being transferred through the lower extremities [68]. The anatomical axes run through the intramedullary canals of both the tibia and the femur

[67]. In this study, the anatomical axes are used for measurement and compared to the 6 degree angle as a normal alignment.

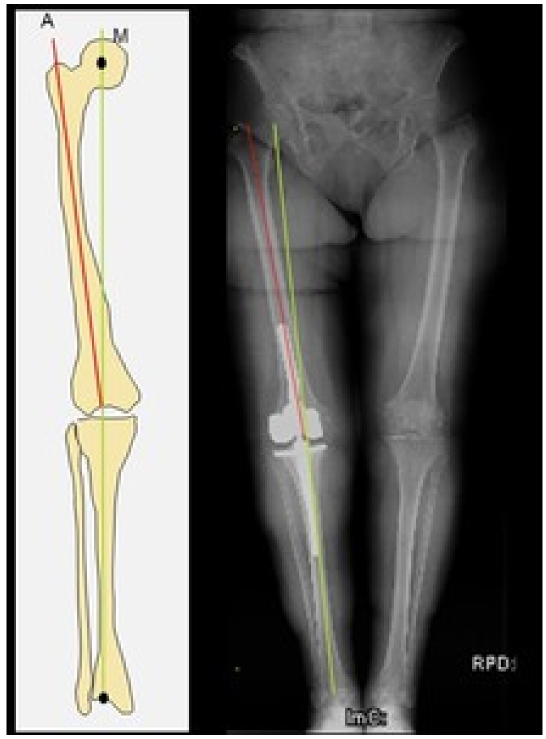

Figure 19: The mechanical axis (M) runs from the center of the femoral head, through the center of the knee, and to the center of the ankle joint. The anatomical axis (A) runs through the intramedullary canal of both the femur and the tibia. Reprinted from [69].

There are demonstrated relationships between obesity and joint complications in the weight-bearing joints of the lower extremity. There are additionally relationships between certain anatomic variables and an increase in joint complications in lower extremities. The objective of this study was to identify the degree to which obesity influences shape variation of the osseous anatomy of the knee joint.

3.2: Methodology

The same patient/image population was used as in Chapters 1 and 2. Using a custom computational algorithm coded in Matlab, measurements collected consisted of anteroposterior depth (AP depth), mediolateral width (ML width), tibial slope, and anatomical alignment.

Anatomical landmarks were identified through the use of seed points and automatic generation of circles. The lateral seed point placement process can be seen in Figure 20 and the AP seed point placement process can be seen in Figure 21.

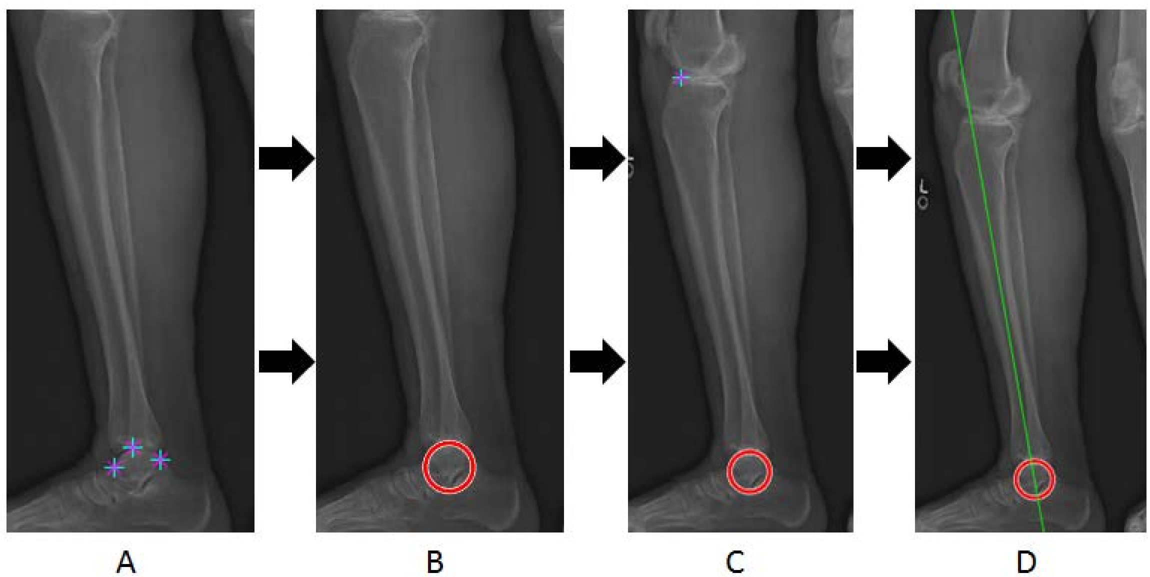

Figure 20: Lateral view of seed placement process. For generation of the tibial anatomical axis, three points were placed on the talar dome (A). From these three points, a circle was automatically generated, with the center corresponding to the distal tibia (B). Another seed point was placed on the tibial condyle (C) marking the proximal point of the tibial axis. A line was generated to connect the proximal tibia to distal tibia, forming the tibial anatomical axis (D).

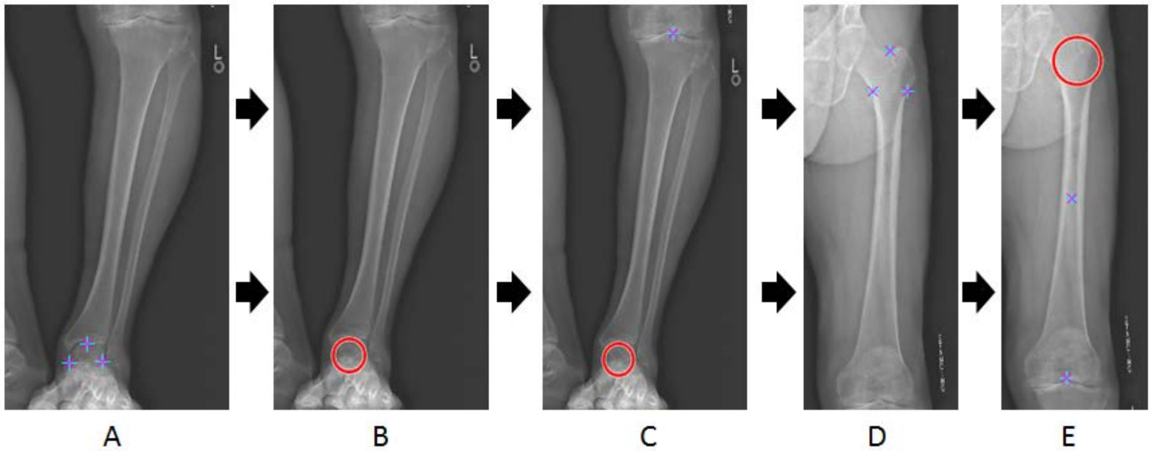

Figure 21: Anteroposterior view of seed placement process. For generation of the tibial anatomical axis, again three points were placed on the talar dome (A). A circle was automatically generated from these points, with the center corresponding to the distal tibia (B). The next seed point was placed on the tibial condyle (C) marking the proximal point of the tibial axis. A line was generated to connect the proximal tibia to distal tibia, forming the tibial anatomical axis. For the generation of the femoral anatomical axis, three points were placed on the greater trochanter, lesser trochanter, and gluteal tuberosity (D). From these three points, a circle was automatically generated with the center marking the proximal point of the femoral axis. Two additional seed points were placed at the tibial condyle and another at the center of the femoral shaft approximately half way along the axis (E). The proximal femoral point was connected to the tibial condyle point marking the femoral anatomical axis.

In measuring the AP depth, ML width, tibial slope, and degree of varus or valgus, axes of origin were created by generating a line through the mechanical axis of the tibia and femur as shown below in Figure 22.

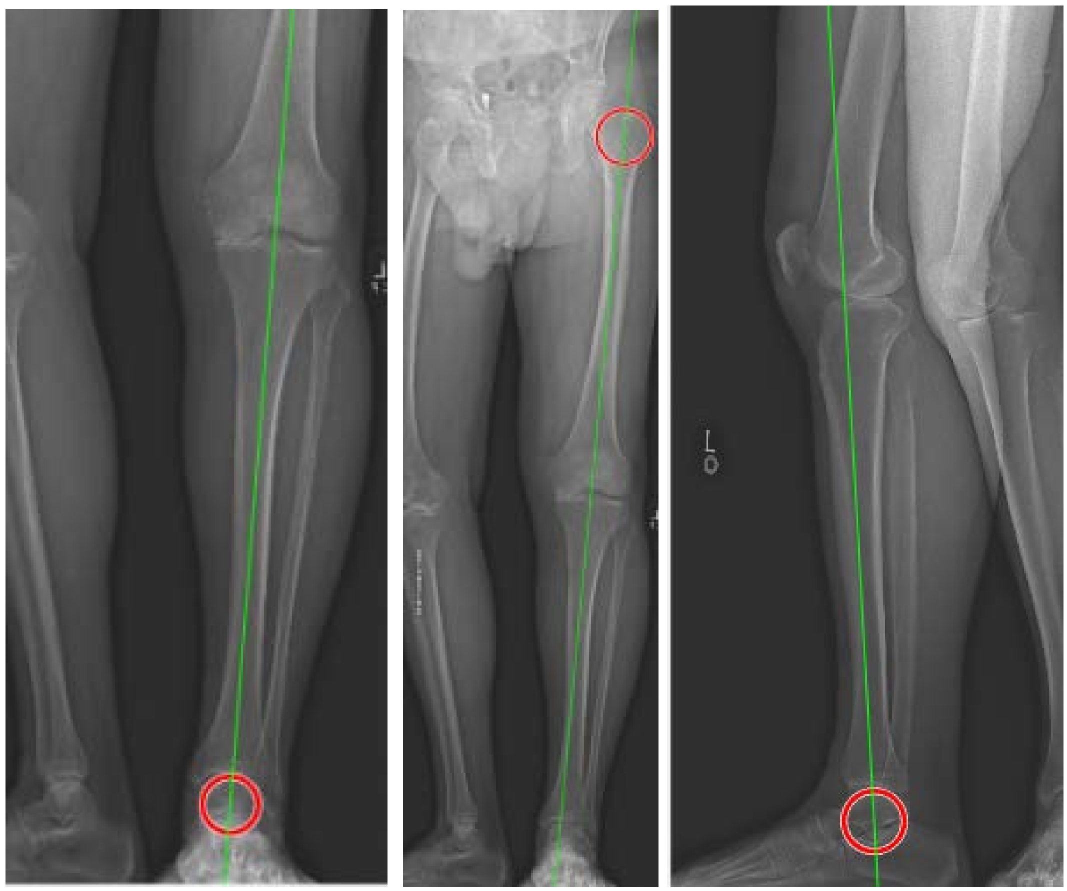

(A) (B) (C)

Figure 22: Screen shots of the MATLAB axis generation interface. (A) Using three seed points on the talus, the red circle was constructed with the center representing the distal point of the tibial axis. Another point was generated at the tibial condyle. The green line shown connects these two points generating the axis of the tibia. (B) Using three seed points placed on the greater trochanter, lesser trochanter, and gluteal tuberosity, the red circle was constructed with the center representing the proximal point of the femoral axis. Another point was generated at the tibial condyle. The green line shown connects these two points generating the axis of the femur. (C) Using three seed points on the talus, the red circle was constructed with the center representing the distal point of the tibial axis. Another point was generated at the tibial condyle. The green line shown connects these two points generating the axis of the tibia.

Once the anatomical axes of the tibia and femur were generated, the measurements for the AP depth, ML width, tibial slope, and degree of varus or valgus were based off these axes as origin. The AP depth was measured as the distance from the most anterior point on the tibia to the most posterior point on the tibia 10mm below the lateral condyle (most TKA remove a minimum of 10mm from the proximal tibia [32]) and perpendicular to the previously generated tibial axis as shown in Figure 24 (A). The ML width was measured as the distance from the most medial point on the tibia to the most lateral point on the tibia, both lying on the line placed 10mm below the lateral condyle as shown in Figure 24 (B). A demonstration of these measurements can be seen below in Figure 23.

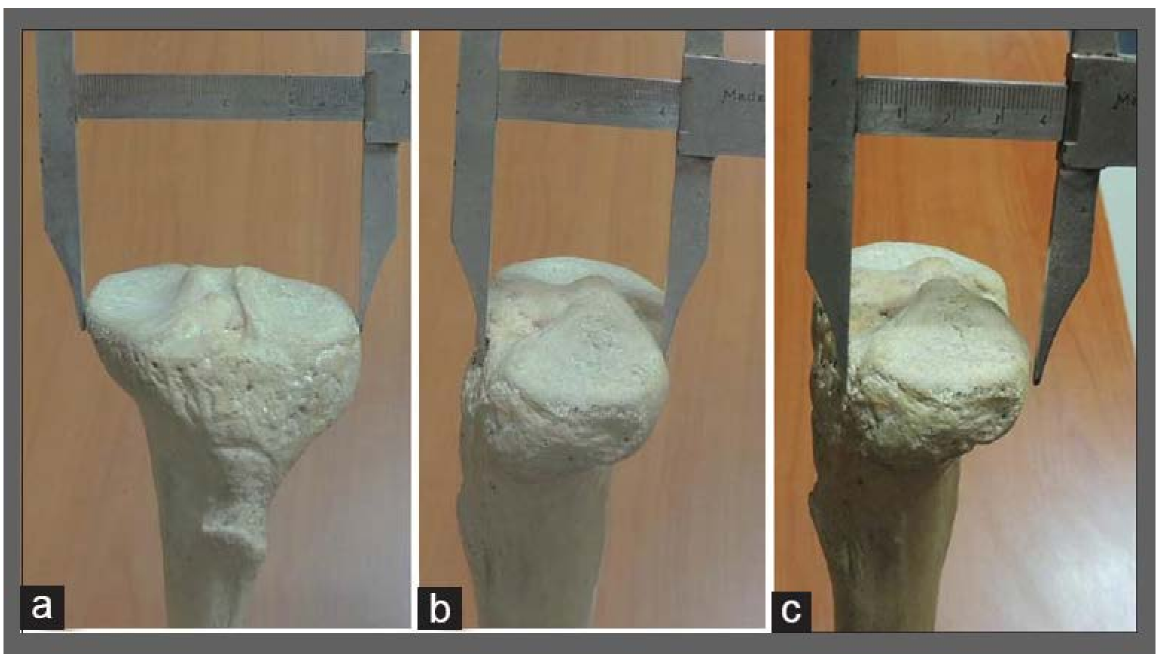

Figure 23: Representation of the measurements for ML width and AP depth. (a) Shows the ML width measurement as the outer two most points on the proximal tibia. (b) Shows a method of measurement for the AP depth that was used in previous studies, but was found not to be as reliable when looking at lateral view radiographs due to the lack of viewing the posterior intercondylar area. (c) Shows the method of measurement that was used in this study, representing the AP depth as the distance from anterior tibia to posterior point of the lateral condyle [70].

The tibial slope was measured as the angle between a line perpendicular to the tibial axis and a line connecting the anterior and posterior points of the lateral condyle as shown in Figure 24 (C). The degree of varus and valgus was measured as the angle between the femoral and tibial axes as shown in Figure 24 (D), using anatomical alignment as a reference. This was compared to a normal value of 5-9 degrees in valgus as opposed to the previously reported 3.3 degrees of varus for a normal lower extremity alignment [71] There have been non-radiographic attempts at measuring varus/valgus alignment, as long-leg radiographs are not always readily available and can be costly, but the radiographic precision still proves to be the gold standard [72].

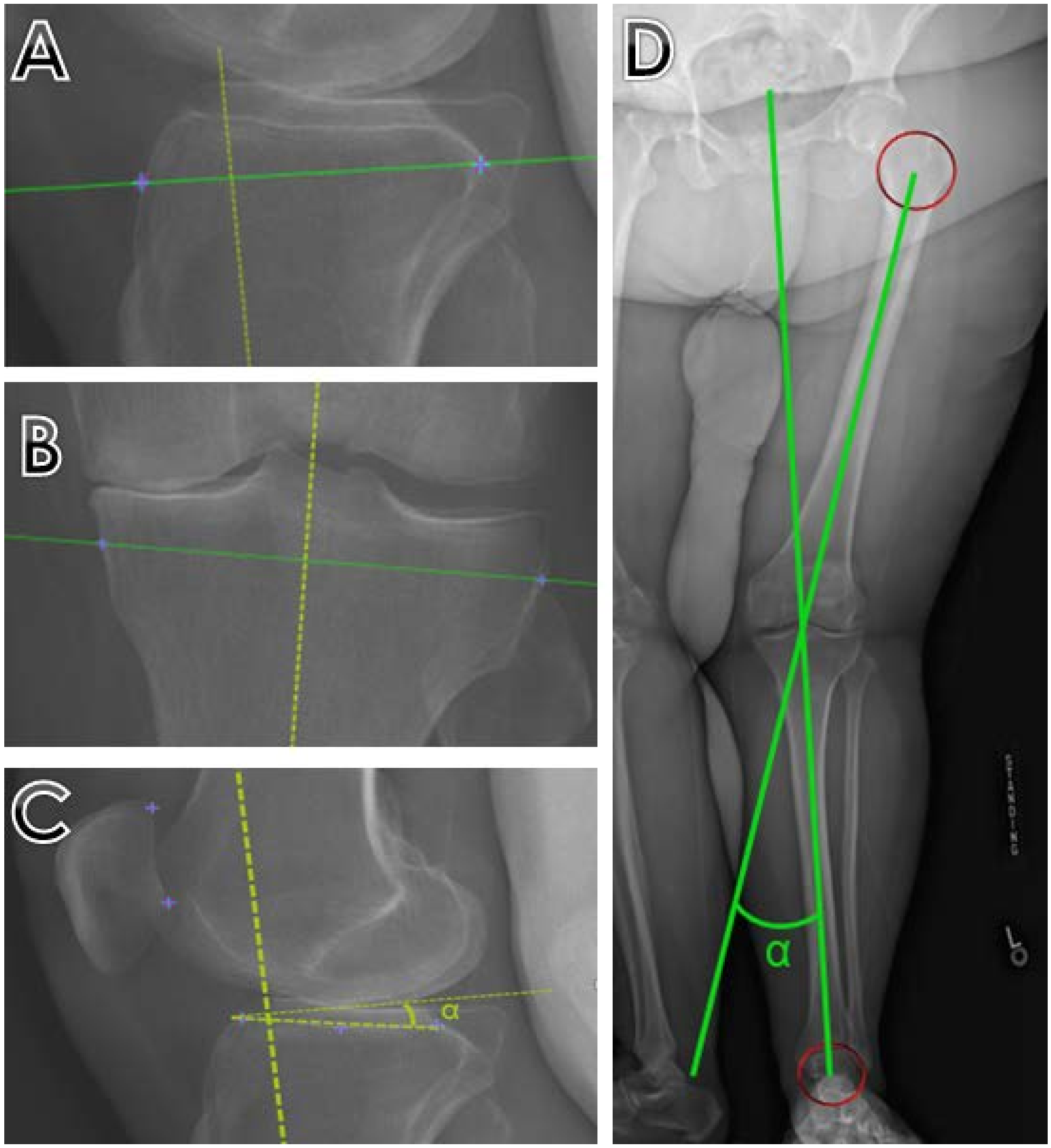

Figure 24: Screen shots of the MATLAB measurement interface. (A) AP depth measured as distance between points on anterior surface of the tibial and posterior surface of the lateral condyle 10mm below the lateral condyle. (B) ML width measured as distance between points on medial and lateral surfaces of the tibia at 10mm below the lateral condyle. (C) Tibial slope measured as the angle between a line created perpendicular to the tibial axis and a line created by two points on the anterior and posterior of the lateral condyle. (D) Degree of varus or valgus measured as the angle between the femoral axis and tibial axis, with α = 0 denoting a straight leg alignment.

Measurements for AP depth, ML width, tibial slope, and degree of varus or valgus were able to be obtained in 229 of the original 231 patients, where two subjects were unable to be completely analyzed due to inadequate radiographic resolution. The measurements were assessed for reproducibility by re-running 15 of the patients, selected at random, a second time and comparing their data to the original measurements in an attempt to reduce intra-observer variability. All length measurements averaged ± 3mm (range, ± 6mm) difference from their original measurement. All varus/valgus measurements averaged ± 0.8 degrees (range, ± 1.4 degrees) difference from their original measurement.

3.3: Results

For both male and female patients, the AP depth did not demonstrate an association with BMI, remaining relatively constant for all subjects. The ML width, in both the male and female populations, tended to demonstrate modest increase in distance with an increase in BMI. However, the ML width was on average 12mm greater in the male population. Similar to AP depth, the tibial slope, which averaged 11.9 degrees for males and 12.9 degrees for females, did not correlate with BMI. No correlation was observed between BMI and varus/valgus alignment of the leg. The average alignment was roughly 0.5 degrees in varus, with a range from 16.7 degrees in valgus to 24.8 degrees in varus. These comparisons are demonstrated in Figure 25-28.

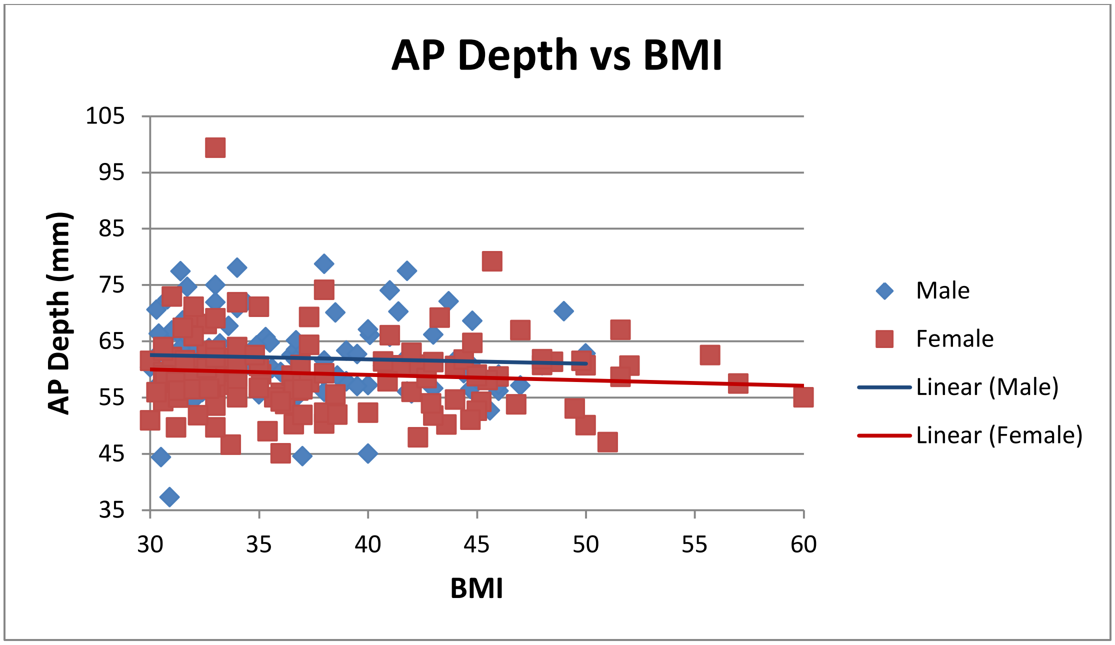

Figure 25: Demonstrates a comparison between AP depth and BMI for males and for females.

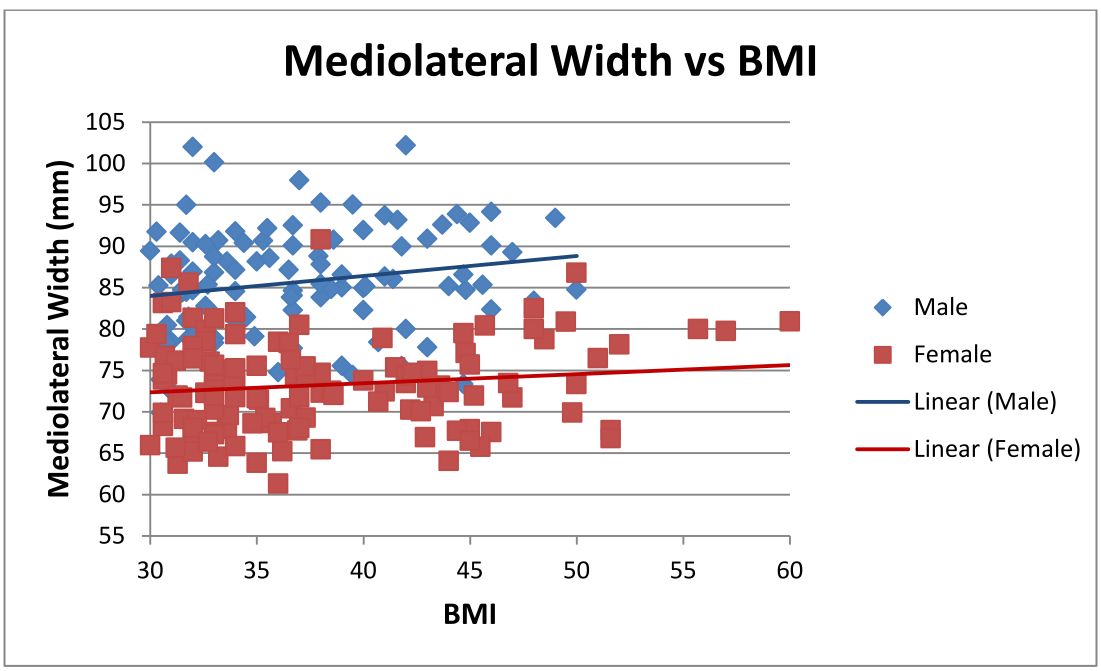

Figure 26: Demonstrates a comparison between ML width and BMI for males and for females.

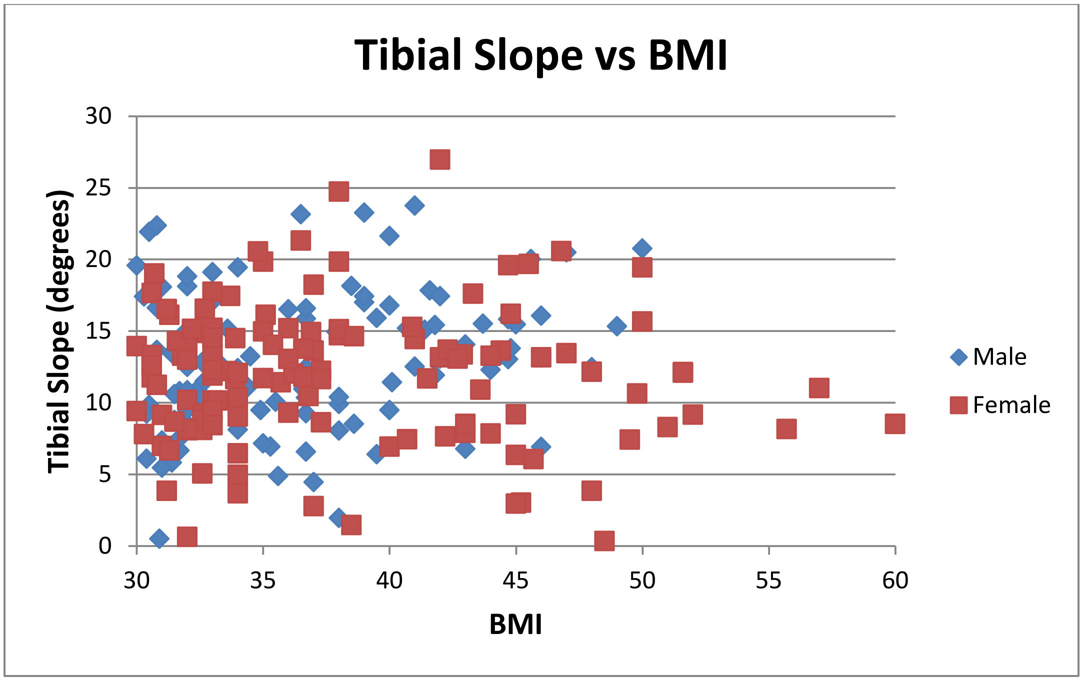

Figure 27: Demonstrates a comparison between tibial slope and BMI for males and for females.

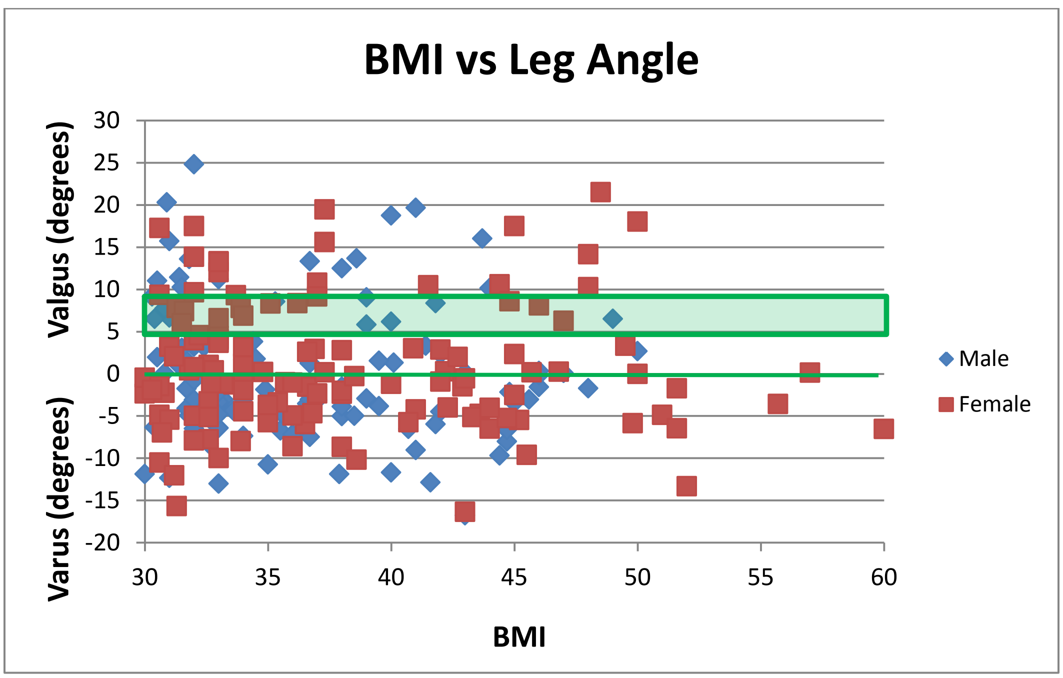

Figure 28: Demonstrates a comparison between varus/valgus alignment and BMI for males and for females with the green box representing normal in reference to the anatomical alignment.

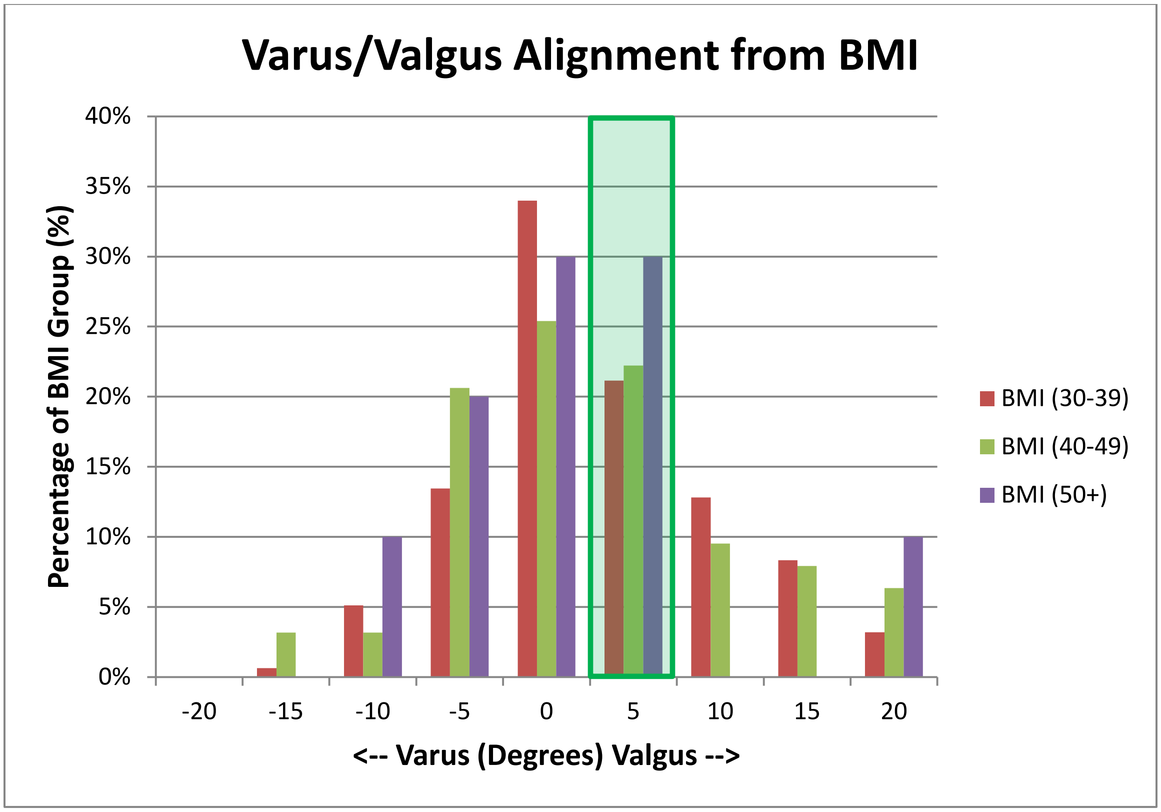

Figure 29: Histogram demonstrating how patients among several BMI groups vary in varus/valgus alignment. The green box represents the normal zone in reference to normal anatomical alignment.

In Figure 29 above, the tibial-femoral joint anatomical alignment distributions for BMIs of 30-49 are similar, but skewed toward varus compared to the normal alignment in the green box. The BMI (50+) group tend to be closer to the normal alignment, however, they are still skewed slightly in varus.

3.4: Discussion

Defining the proximal tibia, the AP depth and ML width gave indications as to possible bony remodeling strategies secondary to increased loading in obese patients. The AP depth was found to be independent upon BMI; however the ML width tended to increase with obesity. It is important to note that an increase in body weight does not necessarily coincide with an increase in osseous size. Precious reports of morphotypes suggest that ectomorphs have large bones and increased fat. This study shows that they do not always correlate with each other. Along with an increasing ML width in obese individuals, previous reports have attributed compensatory increased tibial shaft diameter and increased bone mineral density with increased trabeculae, with helping support the increased loads on obese limbs in accordance with Wolff's law [59] [60] [73]. As stated by Wolff's law, due to changing strains in bone, the osseous structure will remodel in order to support the new demands placed upon the bone. From this, it was not expected that both AP depth and ML width would increase with increasing BMI, but bone mineral density would likely account for this difference in load. Therefore, as expected, AP depth remained fairly constant with increasing BMI, and ML width only increased slightly. Although the bone did not demonstrate compensatory growth in all dimensions, the overall surface area of the tibia did tend to increase. This growth in only the mediolateral direction may be a result of instable gait patterns in obese patients, possibly generating more variability in the mediolateral direction. One interesting observation was that male patients had on average 12mm wider tibias when measured in the ML direction. This is thought to be due in part to the fact that males have a higher center of gravity and therefore needs a wider area to remain stable during daily activity [74]. In implant design, implants can be made patient-specific such as Zimmer's Gender Solution series [62]. Although nearly the same in the AP dimensions, the male femoral component is larger in ML width. The difference in these implants can be seen in Figure 30.

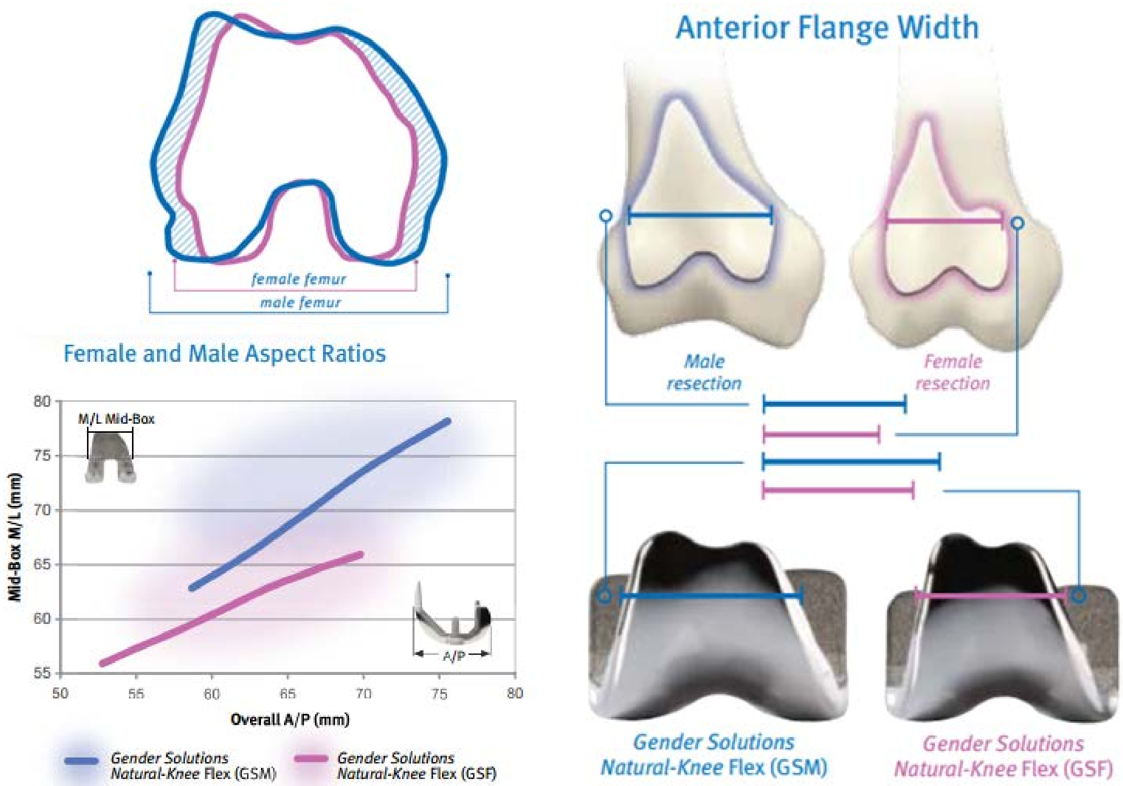

Figure 30: Zimmer Gender Solutions designed a femoral component for TKA with a larger ML width for males. Reprinted from [62].

The tibial slope did not vary significantly among different BMI groups, but averaged 11.9 degrees for males and 12.9 degrees for females, which is slightly greater than the 6-7 degrees of normal patients [63]. It is believed this may be linked to the angle needed to increase range of motion as the tissue on the posterior distal thigh and posterior proximal shank impinge during knee flexion.

No overall relationship was observed between BMI or age, regarding varus/valgus alignment of the leg. The average limb measured only 0.5 degrees of varus, with a range between 16.7 degrees of varus to 24.8 degrees of valgus, compared to the normal 5-9 degrees of valgus for a normal anatomical alignment. However, when categorized into BMI groups, the lower BMIs tended to shift slightly more toward varus alignment. This is different than previous reports that obese individuals tend to drift into valgus as their weight is redistributed to the lateral tibial plateau [75]. It is believed that this shift laterally is not only a response to girth obstruction, but also a response to overloading the medial plateau, thus remodeling to avoid varus collapse of the knee [57].

Similar to the previous section, this investigation has demonstrated correlation between lower extremity shape and body mass index. The measurements made in this study can be used to generate accurate models of lower extremity tibial alignment on a patient specific basis. This is important not only for permitting precise computational assessment of the joint biomechanics in obese patients, but also to predict possible adverse outcomes following TKA. This study considerably expands our knowledge-base of lower extremity alignment and tibial shape adaptation in obese patients. Thus in reference to the long-term goals of the lower extremity model, the osseous geometry is now a known entity.

There were a few limitations on this study. The patient sample size was limited, end-stage OA patients requiring TKA, which made it difficult to extrapolate significant findings. Also, the patient population data was highly clustered in the BMI 30-40 range, limiting the observations at higher BMIs and comparisons to normal patients. A possible cohort to include in future studies that have increased BMI, without OA, may be collegiate athletes. Often times they have healthy, young bones, but qualify with greater BMI due to increased muscle mass. A minor limitation was that a few of the landmarks were difficult to locate due to poor contrast in the images. These patients were eliminated from the study as to not lose data precision, which further limited the sample size.

CHAPTER 4: KNEE CONTACT FORCE ANALYSIS OF EVERYDAY ACTIVITIES IN OBESE PATIENTS: FRAMEWORK GENERATION

4.1: Introduction

As obesity continues to rise, the medical and societal burdens associated with obesity are expected to continue to rise to the fore. Obesity is commonly associated with increased risk of diabetes, cardiovascular disease, stroke, kidney disease, and early morbidity [2] [76]. From 2004 to 2014, obesity in TKA has increased from 54% to 63% and in THA; obesity has increased from 40 to 45% [77]. Obesity appears to be related to the growing trends of revision and infection following TJA [78]. In the realm of biomechanics, obesity places increased stress upon joints. Additionally, the excessive soft tissue envelope in the thigh region in obese patients is postulated to result in aberrant forces and loading conditions. An example of this is the thigh-thigh impingement that has been associated with dislocation in morbidly obese THA patients [79] [80]. This same soft-tissue impingement, along with larger coronal girth, is thought to cause lower extremities to shift toward a valgus alignment [75].

Patient-specific gait can play a role in longevity of implants following TJA. Obese subjects alter their natural gait movements as to account for the increase in body force. The smaller stride length and greater lateral leg movement all enable the subject to decrease the amount of force needed to make the stride possible [81]. They also have been observed to have slower gait, wider stance, and longer stance duration. This longer stance duration is believed to play a role in improving absorption of additive impact imposed by heavier body mass [82]. Obese gait is often altered from normal kinematics, increasing loosening due to increased debris from varying wear patterns [83]. Prior understandings of how obesity impacts joints have been previously investigated, but despite the intuitive nature that obesity influences locomotion and joint loading, this topic has is wholly understudied relative to its relative morbidity burden. In an effort to better understand how obesity affects the weight-bearing joints of the lower extremity; this study compares the knee contact force of individuals with normal and increasing BMI through motion capture analysis of various activities of daily living.

4.2: Methodology

Motion capture took place in the Orthopaedic Gait Analysis Laboratory at the University of Iowa. Motion capture data was collected in an attempt to analyze the joint contact force in the knee of obese patients during gait, sit-to-stand, and stair ascent. Trial runs were set up using the researchers as testing subjects to collect trial data.

4.2.1: Motion Capture

In order to run motion capture analysis on patients, the first step was calibrating the capture space. During this time, the force plates were zeroed. The cameras captured axes by placing a marked, L-bar at the room's origin, followed by sweeping a rigid object with mounted markers to sensitize the cameras to the space. This process can be visualized in Figure 31.

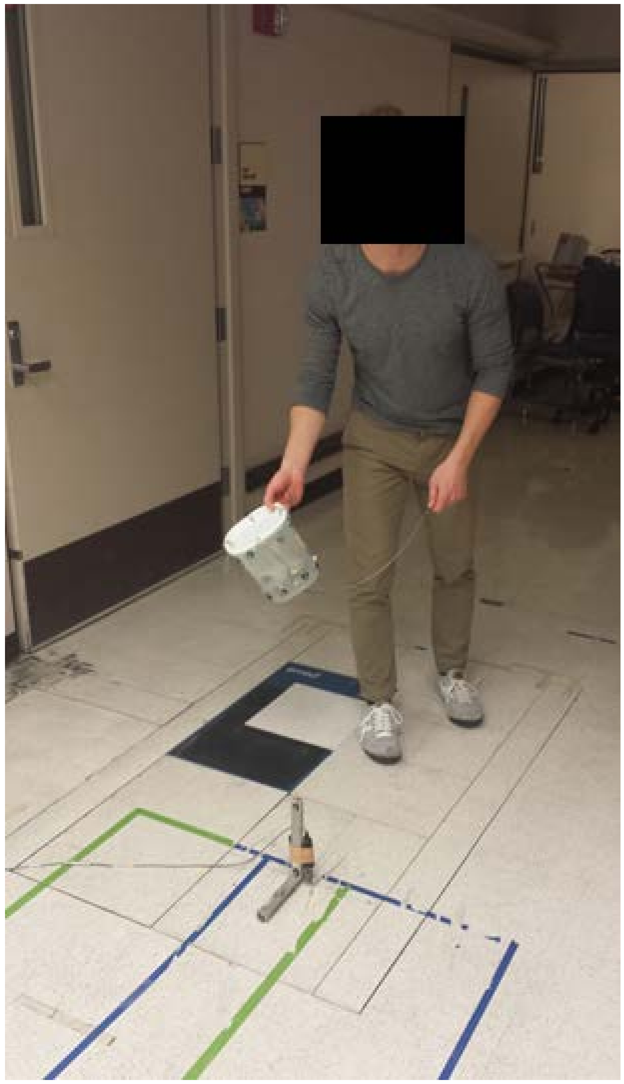

Figure 31: Calibration of capture space with marked L-bar and marked box.

The next step was to set up the markers on the patients. The marker placement was similar to that found in prior reports [84] [85]. A total of 24 infrared emitting diodes (IREDs), affixed in triads, were placed on the subject in groups of three. Starting distally, the first group of three was placed on the lateral surface of the foot, just inferior to the lateral malleolus. The next set was placed along the lateral surface of the shank, just inferior to the halfway point. The next set was placed on the lateral surface of the thigh, slightly distal to the center of the thigh. These first three sets were symmetric on both legs. The markers for the sacrum and cervical portion of the spine were fixed to 5-cm extensions with base plates affixed to the sacrum and C7-vertebrae. The setup can be visualized in Figure 32. These IREDs were placed on segments in locations that attempted to minimize amount of soft tissue between the bone and markers. This would ultimately give the most repeatable data with the minimal variability due to markers moving as a result of soft tissue moving.

Figure 32: Anterior, lateral and posterior view of IRED placement on test subject.

Using the probe seen in Figure 33, anatomical landmarks were digitized relative to segment local coordinate systems while subjects stood in a neutral position to create an anatomical model. Segment principle axes were based on single researcher palpating and probing to digitize the following 22 bony landmarks: sternal notch, inferior sternum, C-7 vertebrae, T-10 vertebrae, and left/right marks for first and fifth metatarsals, lateral malleoli, distal heel, mid-tibia, lateral femoral condyles, mid-thigh, anterior and posterior iliac crests. The probing allowed us to push through some skin and get as close to bone as possible to generate the most reliable landmarks possible [86]. These digitized landmarks are what are later used to drive the AnyBody models.

Figure 33: Probe used in digitizing bony landmarks for anatomical markers.

Kinematic data was collected using an Optotrak motion analysis system (Model 3020, Northern Digital Inc., Waterloo, Ontario, Canada) operating at 60 Hz and filtered at 6 Hz, using a zero phase lag, fourth-order, Butterworth low pass filter. Kinetic data was obtained using a Kistler force plate (Kistler Instruments, Inc., Amherst, NY). The force plate data was sampled at 300 Hz and filtered at 6 Hz, thus providing ground reaction forces. Visual 3D software (C-Motion Inc., Germantown, MD) was used to process lower limb kinematic and kinetic data on the force plates, utilizing a pre-made pipeline command [87] [88]. Once the data was processed in Visual3D, it was output as a .c3d file to be read into AnyBody.

4.2.1.1: Sit-to-Stand

One of the three tasks in the study was a sit-to-stand motion. For this task, the subject was instructed to sit on the bench with their feet comfortably in front of them, evenly distributed to the two force plates. During the standing motion, the subject was to stand up, using as little arm-on-thigh help as possible. This set-up can be visualized in Figure 33 and the Visual3D representation of this can be seen in Figure 35.

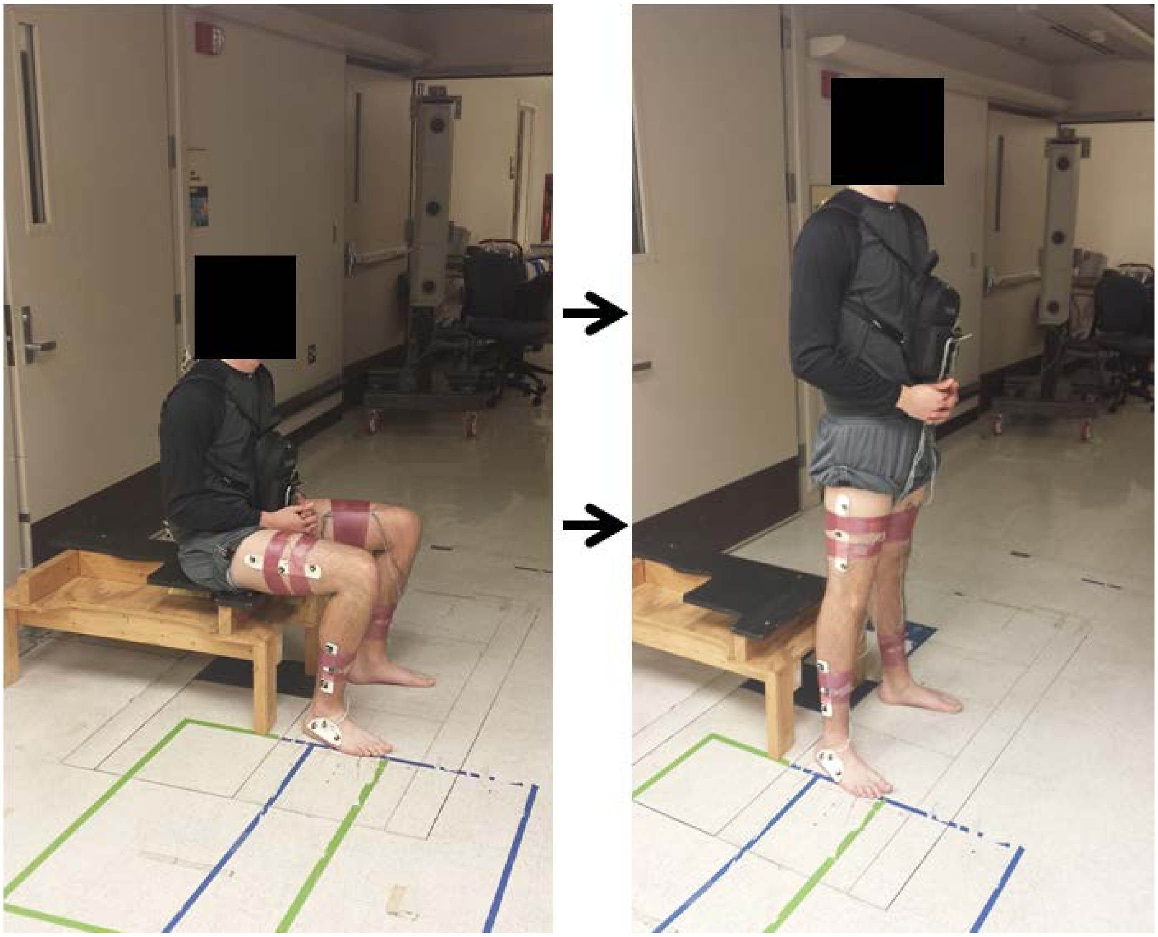

Figure 34: Sit-to-stand set-up for motion capture process.

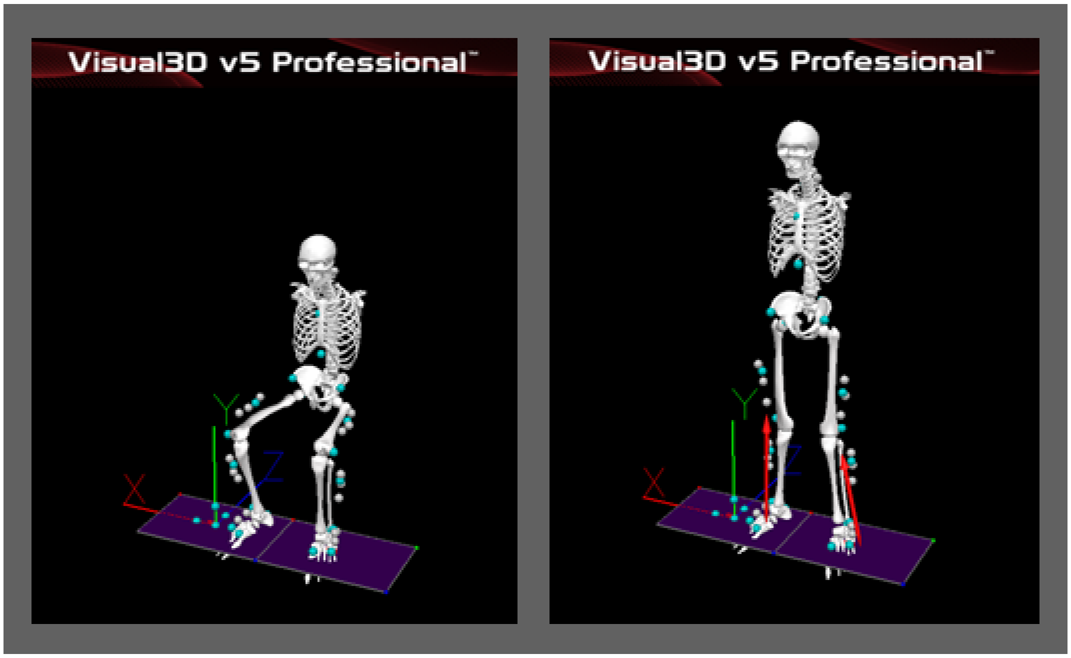

Figure 35: Screenshots of the sit-to-stand task in the Visual3D processer.

4.2.1.2: Gait

Another of the three tasks in the study was a standard gait motion. For this task, the subject was instructed to make a couple of passes, walking over the force plate, until an optimal start point could be marked to ensure a natural stride when contacting the force plates. The subject then walked over the plates for several data collections in order to ensure a clean collection was captured, with foot strike occurring near the center of the force plate. This set-up can be visualized in Figure 36 and the Visual3D representation of this can be seen in Figure 37.

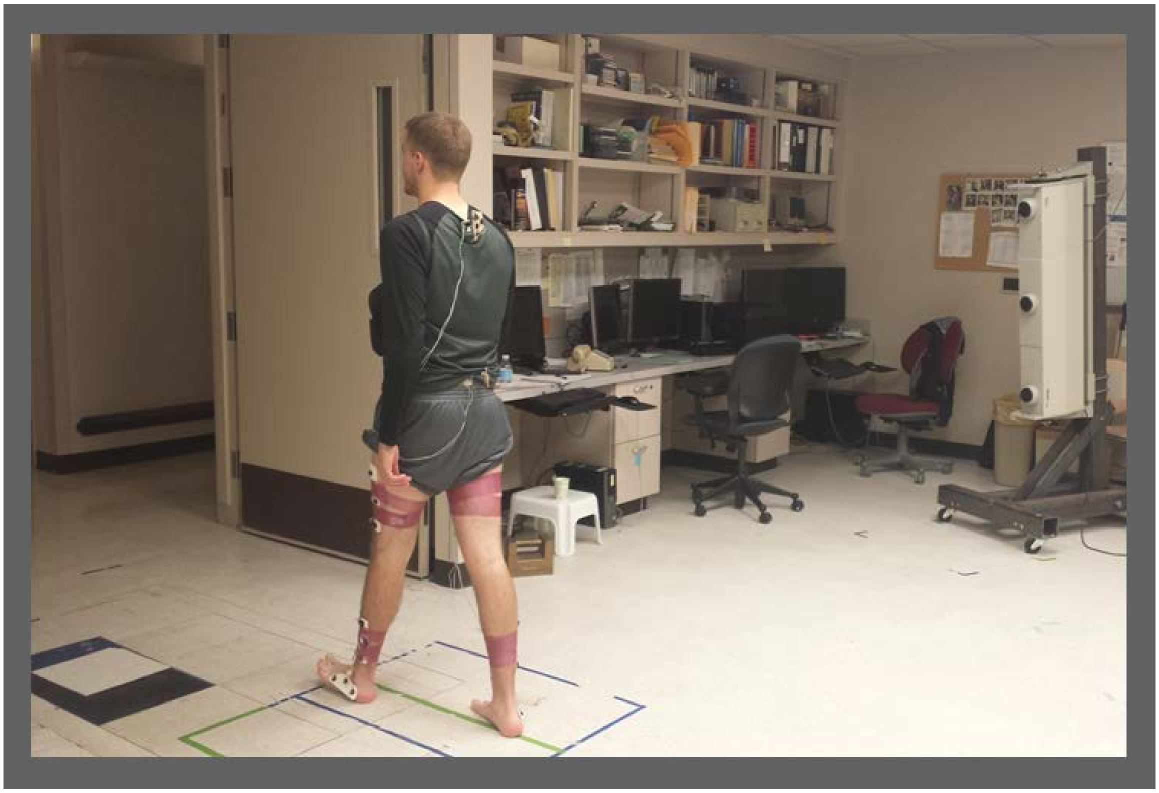

Figure 36: Motion capture set-up for gait analysis with left foot striking force plate.

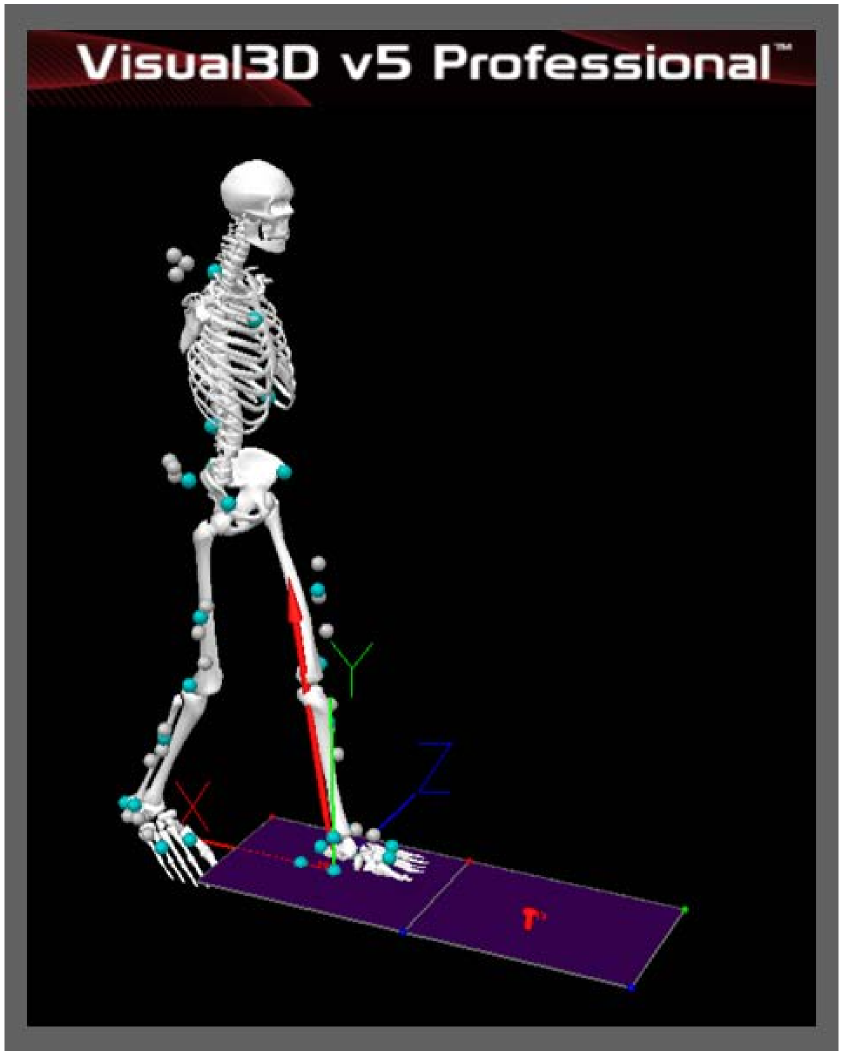

Figure 37: Screenshot of the gait task in the Visual3D processer.

4.2.1.3: Stair Ascent

Another of the three tasks in the study was a stair-climbing motion. For this task, the subject was instructed to make a couple of passes, walking over the force plate and stepping up to the second step, until an optimal start point could be marked to ensure a natural stride when contacting the force plates and step. The subject was instructed to try using the rail as little as possible and if necessary, only to use it as a side-to-side stabilizer. The subject then walked over the plates, and stepped up to the second step for several data collections in order to ensure a clean collection was captured, with foot strike occurring near the center of the force plate. This set-up can be visualized in Figure 38.

Figure 38: Motion capture set-up for stair-climb analysis with left foot on the force plate and right taking the first step up.

During the stair-climb task, only the initial step on the force plate, along with the first step up was part of the force collection. In order to capture this, the stairs unit was built so that its supports were on the sides of the force plate and not on the force plate. The single, lowest step was free moving, apart from the rest of the staircase and was placed entirely on the second of the two force plates in series as shown in Figure 39. This allowed the force generated by the leg and foot to be transmitted through the step, into the force plate.

Figure 39: Close-up view at the step on force plate during the stair-climb motion capture process.

4.2.2: Creation of AnyBody Model

In order to run the motion capture data through AnyBody for analysis, models must be made in AnyBody to align with the anticipated data format. The base model used was based off of the lower-body model created in the AnyBody managed model repository. Many alterations had to be made in order to set up the model to fit each specific task. That process is available in APPENDIX A: ANYBODY MODEL GENERATION.

Once the set-up is done for one file, it can be used for any other c3d file performing the same task. When changing to a different task, the initial positions must be reset to match the initial position of the subject performing the new task. Models generated for use in gait and sit-to-stand can be seen below in Figure 40.

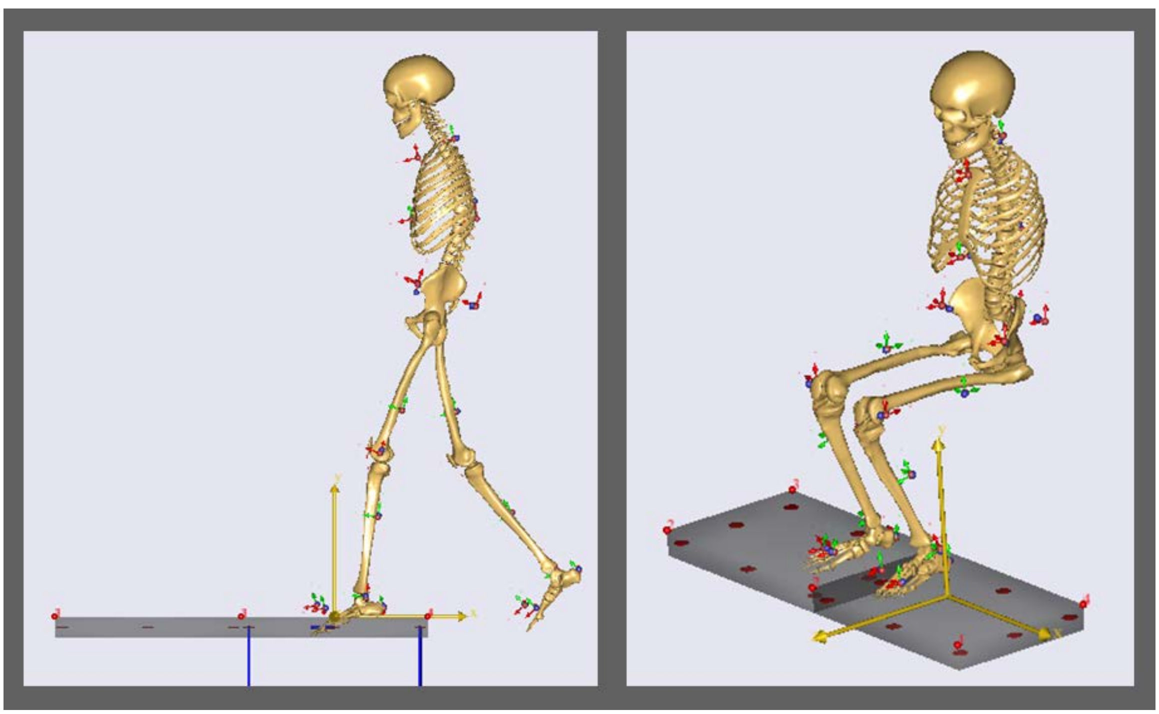

Figure 40: Optimized AnyBody models for gait and sit-to-stand motion.

4.2.3: Running the AnyBody Model

AnyBody runs two separate processes in order to best compute the forces throughout the body. The first of which is an optimization analysis that runs through a series of inner equations and optimization parameters in order to solve for any data in the body that isn't directly given via the motion capture input file. In order to run this, one must simply place a one in front of the optimization of parameters setting, while placing a zero in front of the inverse dynamics setting and press run in the AnyBody main window.

The second process is the inverse dynamics command, which uses the force data from the motion capture file as well as the accelerations of the body parts to calculate forces throughout all of the segments and joints in the body model. In order to run this, one must simply place a zero in front of the optimization of parameters setting, while placing a one in front of the inverse dynamics setting and press run in the AnyBody main window.

4.2.3.1: Gait/Sit-to-Stand

During the inverse dynamics phase of the analysis, a visualization of the generated model walking across the force plates is created with visual feedback on the ground reaction forces, as well as muscle coloration and bulging based on internal computations. An example this in the gait task can be seen below in Figure 41 and an example of the sit-to-stand task can be seen in Figure 42.

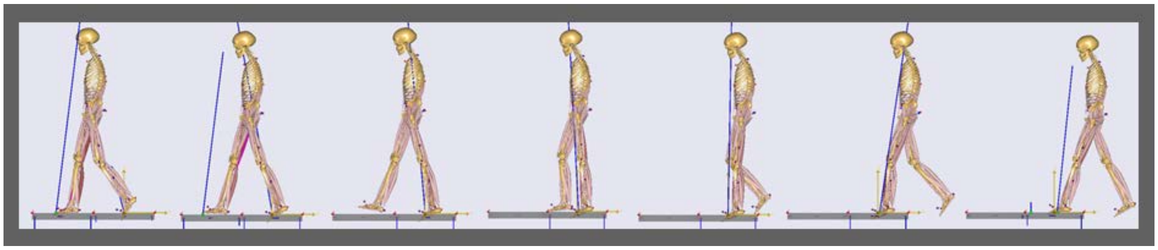

Figure 41: AnyBody model driven by the gait motion capture data, walking from right to left.

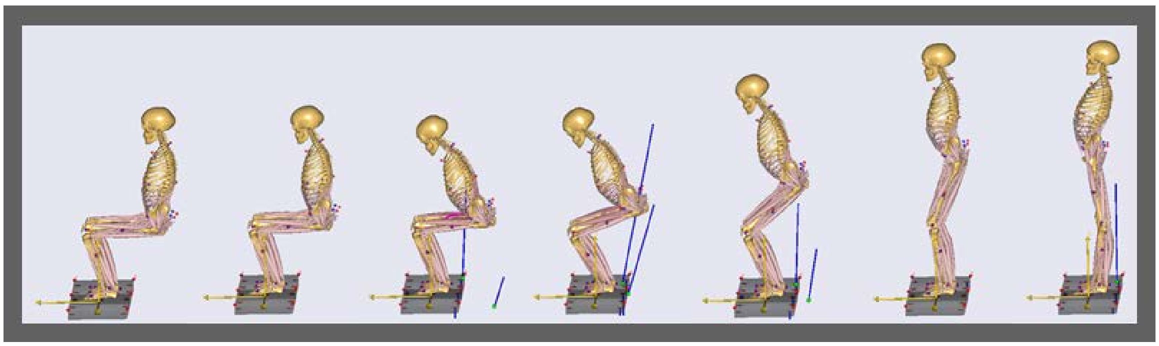

Figure 42: AnyBody model driven by the sit-to-stand motion capture data.

4.3: Results

From AnyBody, one can extract a wide variety of parameters from one single run of the inverse dynamics test. The joint contact force within the knee joint was of particular interest to our group, as it plays a large role in how joints fail and how they can be better designed or implanted. In an attempt to normalize this parameter, it is common to report these forces in terms of percent body weight [89] [90]. As many failures in obese patients occur during motion [91], data was collected in terms of joint contact force as a percentage of body weight, throughout the gait cycle. An example of this data in one of the researchers with a BMI of 23 is shown below in Figure 43. Nearly 4 times body weight is observed at heel strike, dipping slightly before reaching a max of nearly 4.5

times body weight as the opposite leg is about to land, relieving the left leg of most pressure due to body weight.

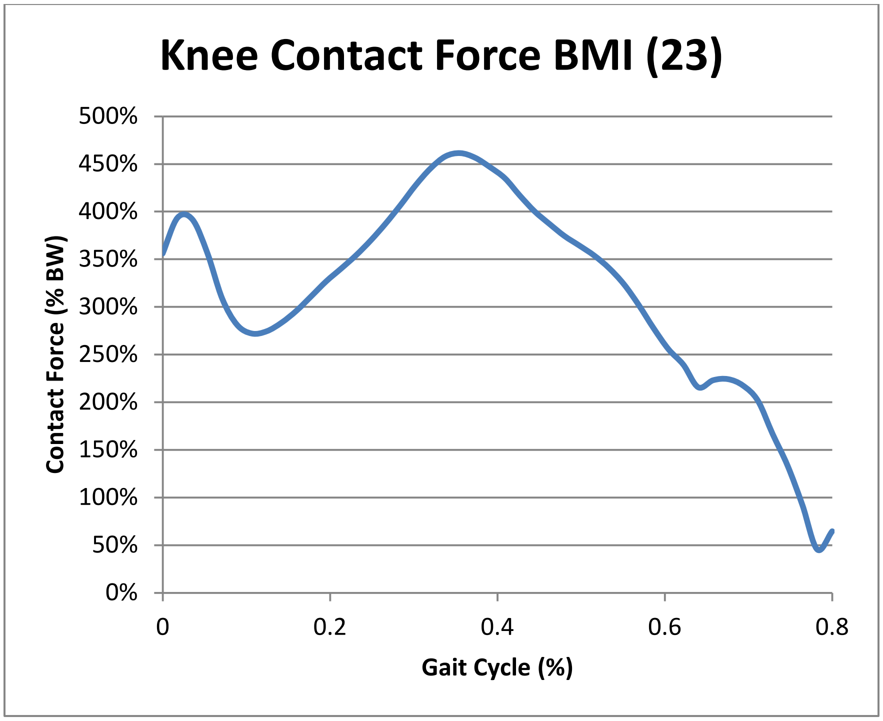

Figure 43: AnyBody results of knee contact force in test subject (BMI 23).

4.4 Discussion

Partial results were able to be obtained for both gait and sit-to-stand tasks. Due to limitations in space and camera function, the gait data was only cleanly collected for the first 80% of the gait cycle, and could not be cleanly collected for the stair ascent task. As mentioned before, during gait, nearly 4 times body weight is observed at heel strike, dipping slightly before reaching a max of nearly 4.5 times body weight as the opposite leg is about to land, relieving the left leg of most pressure due to body weight. AnyBody included a few sets of trial data in the tutorial manual. In Figure 44 below, a comparison is seen between the data collected through the motion capture system on the left with a BMI of 23 (weight (77kg), height (185cm)) and the trial data provided by AnyBody's tutorial on the right with a BMI of 25 (weight (77kg), height (175cm)).

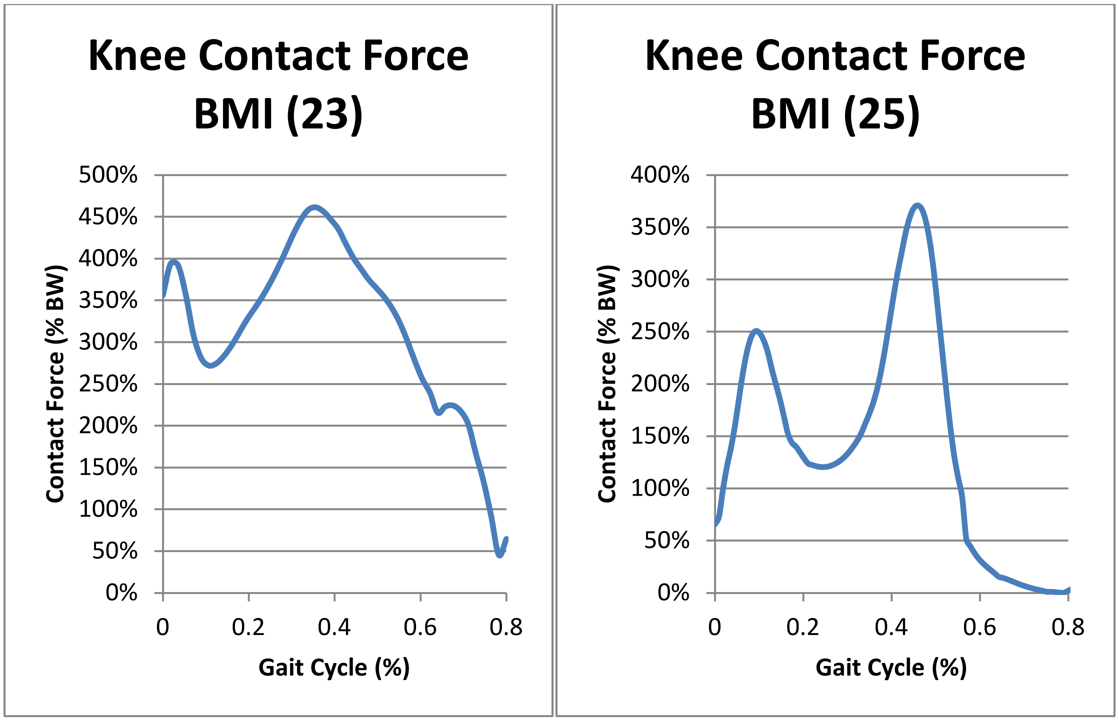

Figure 44: AnyBody results of knee contact force in test subject (BMI 23) and sample subject (BMI 25).

Comparing the test data next to the trial data from AnyBody, one major difference is seen in the overall magnitude of the forces. In the collected data, the forces are greater (higher % BW with same input BW in both data sets), which could be caused by several variables, varying from model simplification, to data collection errors, to a test subject with a build different from the norm. For the same BMI, two test subjects could have very different knee contact forces due to differing joint shapes, differing muscle tones, or differing gait motions. For example, if someone has greater muscle tone than another person of the same BMI, but greater adipose girth, the one with the greater muscle tone will likely have greater knee contact forces due to muscles pulling the joint together.

Another illustrative comparison of the knee contact force of a subject with BMI (23) and BMI (24) can be seen below in Figure 45. The graph on the left (BMI: 23) is again from the data collected via motion capture and run through AnyBody. The graph on the right (BMI: 24) is from a previous study involving the use of AnyBody to calculate knee contact force after TKA, but was conducted in a cadaveric specimen. [92]. The fact that there was new geometry and a new alignment to the joint following TKA will likely play a bit of a role in changing the knee contact force, especially if the knee was aligned for mechanical or for kinematic purposes [93]. Often times the knee joint has more laxity following TKA, thus decreasing the joint's contact forces [94].

More model manipulation and data collection is necessary in the future to generate better and more reliable results.

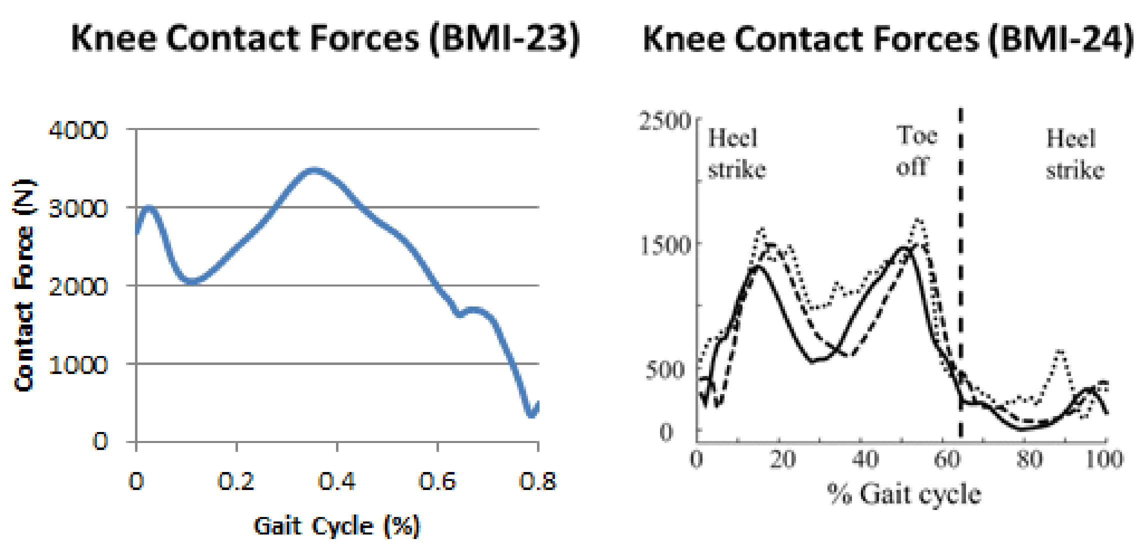

Figure 45: Comparison of knee contact forces to previous experimental study [92].

4.4.1: Future Work

The first item for future work is the setup of the motion capture space. The location of the force plates in the doorway of the motion capture lab made it difficult to place cameras in proper positions at all times. This was extremely detrimental to the data collection of gait because there were many points where a single body segment would get lost for a single frame due to poor camera placement. When running the files through AnyBody, if a single segment is missing during any frame throughout the modeling process, a several errors appear and the file is unable to run. Thus more space in the lab, or better placement of force plates would enhance the data collection capabilities in the future. This loss of data due to poor camera view was also a large issue in the stair ascent task. As the subject approached the stairs, the staircase would block the view of at least one camera, and when climbing the stairs, the subject would climb right out of view. There simply wasn’t enough space in the lab to allow the cameras to view floor to ceiling.

Once all the motion capture space issues are resolved, additional efforts should focus upon marker placement techniques. In obese subjects, there are often motion capture artifacts due to skin motion [95]. The next step for future work would be to run as many subjects, both obese and normal weight, through the three motion tasks. Due to the constraints, there were too few subjects used thus far to have a firm grasp on how accurate the outputs from AnyBody are for this purpose. Although knee contact force is of special interest to surgeons performing TKA, once the process is optimized, AnyBody should be able to provide substantial data, benefiting both surgeons and researchers better appreciate the effects of obesity upon human motion.

One of the mechanisms causing altered joint loading in obese patients may be the alteration of the muscle force due to increased adiposity. Studies have shown that when muscle tissue becomes infused with adipose, muscle fibers become stiff and are able to produce less force [96]. Additional adipose tissue may result in the muscles having altered lines of action, creating altered moment arms around the joints.

Muscle fatigue due to greater loads and overcompensation of previous gait movements can further alter gait. Gluteus medius and soleus muscles are among the most overworked and show greater deviation in obese individuals than their non-obese counterparts [97]. Additionally, obese subjects tend to vary more in the mediolateral direction during the swing phase in order to avoid excess thigh impingement, which causes the muscles to work harder to provide forces over greater distances [98]. Previous reports concluded that obese individuals reorganize their neuromuscular function to produce a gait pattern with less total load on the knee joint [99].

Once enough data is collected to get accurate representations of exactly what forces are present in obese lower extremities, this data can be applied to other research, especially the computational models that are redefining the understanding of lower extremity kinetics in the obese population. However, in reference to the long-term goals of the lower extremity model, the progress of Chapter 4 has now generated a framework for the modelling of the input kinetics and kinematics.

PATH FORWARD

As mentioned in the preface, the long-term objective of the lab is to be able to computationally model total joint replacement in obese subjects. Prior to this study, bone geometry, lower extremity geometry, input kinetics, and input kinematics were unknowns. After completion of this work, the osseous geometry and lower extremity tissue geometry are now known entities. Additionally, a foundation has been constructed to begin in the larger scale input kinetic and kinematic data collection. Along these lines, future work should implement this data collection into the pre-operative work-up for patients. Also, connection with EMG data would increase the capabilities and validation of the future models. Therefore, following successful data acquisition, libraries of benchmark models can be generated and used for future biomechanical research.

APPENDIX A: ANYBODY MODEL GENERATION

The force plate data can be read in many ways, for the sake of the model and force plate data collected, the force plate type needed to be changed to Type3AutoDetection in the main.any>ModelEnvironment.any>ForcePlates.any file, in order to read the Force-x, Force-y, and Force-z components [100]. Running a file requires you to read in the c3d file under the input section of the main.any>TrialSpecificData.any. To select the frames of the c3d file that should be included in the analysis, the number of frames into the file and number of frames from the end of the file must be entered under the time section of main.any>TrialSpecificData.any. Under the anthropometrics section in main.any>TrialSpecificData.any, the body mass and patient height are entered, as well as length of segments they need to be specified; otherwise, the segments will be scaled as functions of body height. AnyBody also uses this data to determine locations of muscle moments and altered lines of action. One is able to set which specific body parameters are to be optimized and which ones are fixed. The next step is setting up the initial position of the body under the initial positions section in main.any>TrialSpecificData.any. Here the rotation of any body segment can be controlled so that the model is able to make an accurate guess as to which c3d markers line up to which body markers during the optimization process. At the bottom of the main.any>TrialSpecificData.any file, the Extra Drivers section gives the ability to add additional drivers to the model if more markers were used in the motion capture process. For the sake of the model used, only the foot and clavicle drivers were used as extra drivers in addition to the pre-set lower body model. The main.any>ModelSetup.any>Input/Markers.any file houses the landmark and driver relations. In here, all of the drivers for the model are paired with the landmarks they represent from the c3d file. AnyBody requires that all of the marker names are 4-letter names that are output by Visual3D.

REFERENCES

[1] W. Shakespeare, Writer, *King Lear.* [Performance]. 1606.

[2] S. B. Heymsfield, "Mechanisms, Pathophysiology, and Management of Obesity," *the New England Journal of Medicine,* vol. 376, no. 3, pp. 254-266, 2017.

[3] T. Stecker, "Prevalence of Obese Patients in a Primary Care Setting," *Obesity,* vol. 14, no. 3, pp. 373-376, 2006.

[4] M. L. Baskin, "Prevalence of obesity in the United States," *Obesity Reviews,* vol. 6, no. 1, pp. 5-7, 2005.

[5] C. Ogden, "Prevalence of Overweight, Obesity, and Extreme Obesity Among," Centers for DiseaseControl anf Prevention, Atlanta, 2010.

[6] R. Iorio, "Orthopaedic Surgeon Workforce and Volume Assessment for Total Hip and Knee Replacement in the United States: Preparing for an Epidemic," *Journal of Bone & Joint Surgery,* vol. 90, no. 7, pp. 1598-1605, 2008.

[7] T. Kelly, "Global burden of obesity in 2005 and projections to 2030," *International Journal of Obesity,* vol. 32, pp. 1431-1437, 2008.

[8] K. M. Flegal, "Prevalence and Trends in Obesity Among US Adults, 1999-2008," *CLINICIAN'S CORNER,* vol. 303, no. 3, pp. 235-241, 2010.

[9] "Health, United States, 2015: With Special Feature on Racial and Ethnic Health Disparities.," National Center for Health Statistics, Hyattsville, MD, 2016.

[10] A. H. Mokdad, "Obesity to Overtake Smoking as Leading Cause of Death," *Journal of the American Medical Association,* 2017.

[11] B. A. Swinburn, "The global obesity pandemic: shaped by global drivers and local environments," *The Lancet,* vol. 378, no. 9793, pp. 804-814, 2011.

[12] S. P. Messier, "Obesity: Effects on Gait in an Osteoarthritic Population.," *Journal of Applied Biomechanics,* vol. 12, no. 2, pp. 161-172, 1996.

[13] S. Messier, "Osteoarthritis of the knee and associated factors of age and obesity: effects on gait.," *Medicine and Science in Sports and Exercise,* vol. 26, no. 12, pp. 1446-52, 1994.

[14] "What is Osteoarthritis?," Arthritis Foundation, [Online]. Available: http://www.arthritis.org/about-arthritis/types/osteoarthritis/what-is-osteoarthritis.php. [Accessed 10 March 2017].

[15] A. J. Teichtahl, "Obesity and Knee Osteoarthritis: New Insights Provided by Body Composition Studies," *Obesity,* vol. 16, no. 2, pp. 232-240, 2008.

[16] Felson, "Obesity and knee osteoarthritis," *Annals of Internal Medicine,* vol. 109, no. 1, pp. 18-24, 1988.

[17] D. Coggon, "Knee osteoarthritis and obesity," *International Journal of Obesity,* vol. 25, pp. 622-627, 2001.

[18] J. J. ANDERSON, "FACTORS ASSOCIATED WITH OSTEOARTHRITIS OF THE KNEE IN," *AMERICAN JOURNAL OF EPIDEMIOLOGY,* vol. 128, no. 1, pp. 179-189, 1988.

[19] B. R, "Role of obesity on the risk for total hip or knee arthroplasty.," *Clinical Orthopedics and Related Research,* vol. 465, pp. 185-188, 2007.

[20] C. K. Ledford, "Percent Body Fat More Associated with Perioperative Risks After Total," *The Journal of Arthroplasty,* vol. 29, no. 2, pp. 150-154, 2014.

[21] C. D. Watts, "Subcutaneous Fat Thickness Is Associated With Early Reoperation and Infection After Total Knee Arthroplasty in Morbidly Obese Patients," *The Journal of Arthroplasty,* vol. 31, no. 8, pp. 1788-1791, 2016.

[22] J. Foran, "The Outcome of Total Knee Arthroplasty in Obese Patients," *Journal of Bone & Joint Surgery,* vol. 86, no. 8, pp. 1609-1615, 2004.

[23] S. Salih, "Obesity, knee osteoarthritis and knee arthroplasty: a review," *BMC Sports Science, Medicine & Rehabilitation,* vol. 5, pp. 1-6, 2013.

[24] M. HA, "The origin of submicron polyethylene wear debris in total hip arthroplasty.," *Clinical Orthopedics & Related Research,* vol. 311, pp. 3-20, 1995.

[25] D. PF, "Metal versus polyethylene wear particles in total hip replacements. A review.," *Clinical Orthopedics & Related Research,* vol. 329, pp. 206-216, 1996.

[26] "Train according to your body type," Elodiepuraye Fitness, 24 September 2015. [Online]. Available: https://elodiepuraye.wordpress.com/2015/09/24/train-according-to-your-body-type-entrainez-vous-en-fonction-de-votre-morphotype/. [Accessed 10 March 2017].

[27] S. Gesta, "Developmental Origin of Fat: Tracking Obesity to Its Source," *Cell,* vol. 131, no. 2, pp. 242-256, 2007.

[28] J. Bellemans, "Both Morphotype and Gender Influence the Shape of the Knee," *Clin Orthop Relat Res,* vol. 468, pp. 29-36, 2010.

[29] W. Park, "Body shape analyses of large persons in South Korea," *Ergonomics,* vol. 56, no. 4, pp. 692-706, 2013.

[30] T. Illés, "The EOS™ imaging system and its uses in daily orthopaedic practice," *International Orthopaedics,* vol. 36, no. 7, pp. 1325-1331, 2012.

[31] J. Blackburne, "A new method of measuring patellar height," *The Bone & Joint Journal,* Vols. 59-B, no. 2, pp. 241-241, 1977.

[32] J. M. Leone, "Osteotomy About the Knee: American Perspective," in *Insall & Scott Surgery of the Knee,* Philidelphia, Elsevier Inc., 2012, pp. 910-925.

[33] R. Halır, "NUMERICALLY STABLE DIRECT LEAST SQUARES," 1998.

[34] A. Fitzgibbon, "Direct Least Square Fitting of Ellipses," *PATTERN ANALYSIS AND MACHINE INTELLIGENCE,* vol. 21, no. 5, 1999.

[35] "General Equation of an Ellipse," Math Open Reference, 2011. [Online]. Available: http://www.mathopenref.com/coordgeneralellipse.html. [Accessed 10 March 2017].

[36] W. o. t. A. A. o. H. a. K. S. (. E. B. Committee, "Obesity and Total Joint Arthroplasty : A Literature Based Review," *The Journal of Arthroplasty,* vol. 28, no. 5, pp. 714-721, 2013.

[37] J. R. Martin, "Morbid Obesity and Total Knee Arthroplasty: A Growing Problem," *Journal of the American Academy of Orthopaedic Surgeons,* vol. 25, no. 3, pp. 188-194, 2017.

[38] A. AK, "Total knee replacement in morbidly obese patients. Results of a prospective, matched study.," *Journal of Bone and Joint Surgery,* vol. 88, no. 10, pp. 1321-1326, 2006.

[39] M. Núñez, "Good Quality of Life in Severely Obese Total Knee Replacement Patients: A Case-Control Study," *Obesity Surgery,* vol. 21, no. 8, pp. 1203-1208, 2011.

[40] M. Callanan, "The John Charnley Award: risk factors for cup malpositioning: quality improvement through a joint registry at a tertiary hospital," *Clinical Orthopedics Related Research*, vol. 99, no. 1, p. 45, 2010.

[41] Y. D. Kamat, "Total Knee Replacement in the Obese Patient: Comparing Computer Assisted and Conventional Technique," *The Scientific World Journal,* vol. 2014, pp. 1-5, 2014.

[42] F. Zhang, "Factors associated with meniscal body extrusion on knee MRI in overweight and obese women," *Osteoarthritis and Cartilage*, pp. 1-6, 2016.

[43] A. MP, "Increased aseptic tibial failures in patients with a BMI >=35 and well-aligned total knee arthroplasties.," *The Journal of Arthroplasty,* vol. 30, no. 12, pp. 2181-2184, 2015.

[44] W. ER, "Effect of Body Mass Index on Complications and Reoperations After Total Hip Arthroplasty.," *The Journal of Bone and Joint Surgery,* vol. 98, no. 3, pp. 169-179, 2016.

[45] A. HM, "The effect of BMI on 30 day outcomes following total joint arthroplasty.," *Journal of Arthroplasty,* vol. 30, no. 7, pp. 1113-1117, 2015.

[46] F. T., "Thickness of Subcutaneous Fat as a Strong Risk Factor for Wound Infections in Elective Colorectal Surgery: Impact of Prediction Using Preoperative CT," *Digestive Surgery,* vol. 27, no. 4, pp. 331-335, 2010.

[47] A. I. Mehta, "Thickness of Subcutaneous Fat as a Risk Factor for," *THE JOURNAL OF BONE AND JOINT SURGERY*, vol. 95, pp. 323-328, 2013.

[48] W. G, "The effect of body mass index on the risk of post-operative complications during the 6 months following total hip replacement or total knee replacement surgery.," *Osteoarthritis and Cartilage*, vol. 22, no. 7, pp. 918-927, 2014.

[49] L. LM, "Relationship between knee anthropometry and surgical time in total knee arthroplasty in severely and morbidly obese patients: a new prognostic index of surgical difficulty.," *Obesity Surgery,* vol. 18, no. 9, pp. 1149-1153, 2008.

[50] S. N, "Mini-subvastus approach for total knee arthroplasty in obese patients.," *Indian Journal of Orthopedics*, vol. 44, no. 3, pp. 292-299, 2010.

[51] I. Y, "Large thigh girth is a relative contraindication for the subvastus approach in primary total knee arthroplasty.," *The Journal of Arthroplasty,* vol. 22, no. 4, pp. 569-573, 2007.

[52] G. P. Pappas, "Magnetic Resonance Imaging of Asymptomatic Knees in Collegiate Basketball Players: The Effect of One Season of Play," *Clinical Journal of Sport Medicine,* vol. 26, no. 6, pp. 483-489, 2016.

[53] G. Strutzenberger, "Uphill walking: Biomechanical demand on the lower extremities of obese adolescents," *Gait & Posture,* vol. 54, pp. 20-26, 2017.

[54] Z. F. Lerner, "Compressive and shear hip joint contact forces are affected by pediatric obesity during walking," *Journal of Biomechanics,* vol. 49, no. 9, pp. 1547-1553, 2016.

[55] F. E. Donaldson, "Prediction of contact mechanics in metal-on-metal Total Hip Replacement for parametrically comprehensive designs and loads," *Journal of Biomechanics*, vol. 48, no. 10, pp. 1828-1835, 2015.

[56] G. Matsoukas, "Design Optimization of a Total Hip Prosthesis for Wear Reduction," *Journal of Biomechanical Engineering,* vol. 131, no. 5, pp. 1-12, 2009.

[57] T. K. Fehring, "Catastrophic Varus Collapse of the Tibia in Obese Total Knee Arthroplasty," *The Journal of Arthroplasty,* pp. 1-5, 2017.

[58] E. Radin, "ROLE OF MECHANICAL FACTORS IN PATHOGENESIS OF PRIMARY OSTEOARTHRITIS," *The Lancet*, vol. 299, no. 7749, pp. 519-522, 1972.

[59] H. M. Frost, "Wolff's Law and bone's structural adaptations to mechanical usage: an overview for clinicians.," *The Angle Orthodontist,* vol. 64, no. 3, pp. 175-188, 1994.

[60] K. I. Harrington, "Size and Shape Differences in the Distal Femur and Proximal Tibia between Normal Weight and Obese American Whites," *Journal of Forensic Sciences,* vol. 30, no. S1, pp. S32-S38, 2015.

[61] C. B. Ruff, "Long Bone Articular and Diaphyseal Structure in OldWorld Monkeys and Apes. II: Estimation of Body Mass," *American Journal of Physical Anthropology,* vol. 120, pp. 16-37, 2003.

[62] "Zimmer®," Zimmer, Inc., 2009. [Online]. Available: http://www.zimmer.com/content/dam/zimmer-web/documents/en-GB/pdf/medical-professionals/knee/Zimmer-Gender-Solutions-Natural-Knee-Flex-System-Brochure-97-5416-001-00-Rev-111-2009.pdf. [Accessed 15 March 2017].

[63] S. Matsuda, "Posterior tibial slope in the normal and varus knee.," *The American Journal of Knee Surgery,* vol. 12, no. 3, pp. 165-8, 1999.

[64] E. Hohmann, "Closing or Opening Wedge High Tibial Osteotomy: Watch Out for the Slope," *Operative Techniques in Orthopaedics,* vol. 17, no. 1, pp. 38-45, 2007.

[65] J. R. Giffin, "Effects of Increasing Tibial Slope on," *American Journal of Sports Medicine,* vol. 32, no. 2, pp. 376-382, 2004.

[66] H. DS, "Total joint arthroplasty of the knee.," *Clinical Orthopedics and Related Research,* vol. 192, pp. 23-33, 1985.

[67] J. J. Cherian, "Mechanical, Anatomical, and Kinematic Axis in TKA: Concepts and Practical Applications," *Current Reviews in Musculoskeletal Medicine,* vol. 7, no. 2, pp. 89-95, 2014.

[68] C.-F. Luo, "Reference axes for reconstruction of the knee," *The Knee,* vol. 11, no. 4, pp. 251-257, 2004.

[69] J. A. Arman, "Imaging findings in knee replacement. How can I help the surgeon?," in *ECR 2016*, Madrid, 2016.

[70] C. Gupta, "A morphometric study of the proximal end of the tibia in South Indian population with its clinical implications," *Saudi Journal of Sports Medicine,* vol. 15, no. 2, pp. 166-169, 2015.

[71] G. Maderbacher, "Lower Limb Anatomy and Alignment Affect Natural Tibiofemoral Knee," *The Journal of Arthroplasty*, vol. 31, pp. 2038-2042, 2016.

[72] K. GIBSON, "Measurement of Varus/Valgus Alignment in Obese," *Arthritis Care & Research,* vol. 62, no. 5, pp. 690-696, 2010.

[73] A. L. Evans, "Bone Density, Microstructure and Strength in Obese and Normal Weight Men and Women in Younger and Older Adulthood," *Journal of Bone and Mineral Research,* vol. 30, no. 5, pp. 920-928, 2015.

[74] S. Gambino, The Physics Factbook, Brooklyn: Glenn Elert, 2006.

[75] J. Sun, "Finite element analysis of the valgus," *BioMedical Engineering OnLine,* vol. 15, no. 158, pp. 309-321, 2016.

[76] E. Viguiliouk, "Can pulses play a role in improving cardiometabolic health? Evidence from systematic reviews and meta-analyses," *Annals of the New York Academy of Sciences*, pp. 1-15, 2017.

[77] J. George, "Administrative Databases Can Yield False Conclusions—An Example of Obesity in Total Joint Arthroplasty," *The Journal of Arthroplasty,* pp. 1-5, 2017.

[78] J. George, "Obesity Epidemic: Is Its Impact on Total Joint Arthroplasty Underestimated? An Analysis of National Trends," *Clinical Orthopaedics and Related Research,* pp. 1-9, 2017.

[79] J. M. Elkins, "Morbid Obesity May Increase Dislocation in Total Hip Patients: A Biomechanical Analysis," *Clinical Orthopaedics and Related Research,* vol. 471, no. 3, pp. 971-980, 2013.

[80] T. D. Brown, "Impingement and Dislocation in Total HIP Arthroplasty: Mechanisms and Consequences," *Iowa Orthopedic Journal,* vol. 34, pp. 1-15, 2014.

[81] P. P. Lai, "Three-dimensional gait analysis of obese adults," *Clinical Biomechanics,* vol. 23, no. S1, pp. S2-S6, 2008.

[82] S.-u. Ko, "Characteristic gait patterns in older adults with obesity—Results from the Baltimore Longitudinal Study of Aging," *Journal of Biomechanics,* vol. 43, no. 6, pp. 1104-1110, 2010.

[83] M. M. Ardestani, "Prediction of Polyethylene Wear Rates from Gait Biomechanics and Implant Positioning in Total Hip Replacement," *Clinical Orthopaedics and Related Research,* pp. 1-6, 2017.

[84] B. Singh, "Biomechanical loads during common rehabilitation exercises in obese individuals.," *International Journal of Sports Physical Therapy,* vol. 10, no. 2, pp. 189-196, 2015.

[85] Z. F. LERNER, "Effects of an Obesity-Specific Marker Set on Estimated Muscle and Joint Forces in Walking," *Medicine & Science in Sports & Exercise,* vol. 46, no. 6, pp. 1261-1267, 2014.

[86] K. D. Huffman, "Increased hip abduction in high body mass index subjects during sit-to-stand," *Gait & Posture,* vol. 41, no. 2, pp. 640-645, 2015.

[87] B. Singh, "Changes in Gait over a 30-min Walking Session in Obese Females," *Medicine & Science in Sports & Exercise,* vol. 49, no. 3, pp. 555-562, 2017.

[88] B. Singh, "Do fitness and fatigue affect gait biomechanics in overweight and obese children?," *Gait & Posture,* vol. 50, pp. 190-195, 2016.

[89] D. J. Saxby, "Tibiofemoral contact forces during walking, running and sidestepping," *Gait & Posture,* vol. 49, pp. 78-85, 2016.

[90] F. Fraysse, "A method for concise reporting of joint reaction forces orientation during gait," *Journal of Biomechanics,* vol. 49, no. 14, pp. 3538-3542, 2016.

[91] D. D. Bohl, "What Is the Timing of General Health Adverse Events That Occur," *Clinical Orthopedics and Related Research,* pp. 1-8, 2017.

[92] Y. Jung, "Intra-Articular Knee Contact Force Estimation During Walking Using Force-Reaction Elements and Subject-Specific Joint Model," *Journal of Biomechanical Engineering,* vol. 138, no. 2, pp. 1-9, 2016.

[93] S. Nakamura, "The effects of kinematically aligned total knee arthroplasty on stress at the medial tibia," *Bone & Joint Research,* vol. 6, no. 1, pp. 43-51, 2017.

[94] W. A. Manning, "Tibiofemoral forces for the native and post-arthroplasty knee: relationship to maximal laxity through a functional arc of motion," *Knee Surgery, Sports Traumatology, Arthroscopy,* pp. 1-9, 2016.

[95] S. Corazza, "A Markerless Motion Capture System to Study Musculoskeletal Biomechanics: Visual Hull and Simulated Annealing Approach," *Annals of Biomedical Engineering,* vol. 34, no. 6, pp. 1019-1029, 2006.

[96] H. Rahemi, "The effect of intramuscular fat on skeletal muscle mechanics: implications for the elderly and obese," *Journal of the Royal Society Interface,* vol. 12, no. 109, pp. 1-8, 2015.

[97] Z. F. Lerner, "Effects of Obesity on Lower Extremity Muscle Function During Walking at Two Speeds," *Gait Posture,* vol. 39, no. 3, pp. 978-984, 2014.

[98] A. G. Sutherland, "Abductor weakness and stresses around acetabular components of total hip arthroplasty: a finite element analysis," *International Orthopedics,* vol. 23, no. 5, pp. 275-278, 1999.

[99] P. DeVita, "Obesity is not associated with increased knee joint torque and power during level walking," *Journal of Biomechanics,* vol. 36, no. 9, p. 1355–1362, 2003.

[100] *Motion Lab Systems User Guide,* Baton Rouge: Motion Lab Systems Inc., 2008.